Weierstraß-Institut

für Angewandte Analysis und Stochastik

Leibniz-Institut im Forschungsverbund Berlin e. V.

Divergence-free reconstruction operators for pressure-robust Stokes discretizations with continuous pressure finite elements

Philip L. Lederer[1], Alexander Linke[2], Christian Merdon[2], Joachim Schöberl[1]

submitted: August 17, 2016

[1] Institute for Analysis und Scientific Computing
    Wiedner Hauptstr. 8-10/101
    1040 Wien, Austria
    email: philip.lederer@tuwien.ac.at
        joachim.schoeberl@tuwien.ac.at

[2] Weierstrass Institute
    Mohrenstr. 39
    10117 Berlin, Germany
    email: alexander.linke@wias-berlin.de
        christian.merdon@wias-berlin.de

No. 2288

Berlin 2016

Abstract. Classical inf-sup stable mixed finite elements for the incompressible (Navier–)Stokes equations are not pressure-robust, i.e., their velocity errors depend on the continuous pressure. However, a modification only in the right hand side of a Stokes discretization is able to reestablish pressure-robustness, as shown recently for several inf-sup stable Stokes elements with discontinuous discrete pressures. In this contribution, this idea is extended to low and high order Taylor–Hood and mini elements, which have continuous discrete pressures. For the modification of the right hand side a velocity reconstruction operator is constructed that maps discretely divergence-free test functions to exactly divergence-free ones. The reconstruction is based on local $H(\text{div})$-conforming flux equilibration on vertex patches, and fulfills certain orthogonality properties to provide consistency and optimal a-priori error estimates. Numerical examples for the incompressible Stokes and Navier–Stokes equations confirm that the new pressure-robust Taylor–Hood and mini elements converge with optimal order and outperform significantly the classical versions of those elements when the continuous pressure is comparably large.

1. Introduction and notation.

1.1. Introduction. The classical Taylor–Hood element [42, 19, 31], its higher order extensions [13] and the classical mini element [1, 19] are among the most popular discretizations for the incompressible Navier–Stokes equations, since they are easy to implement, fulfill a discrete LBB condition and converge with optimal order. Nevertheless they suffer from a common lack of robustness: since they use continuous discrete pressures, they relax the divergence constraint and are thus not pressure-robust [23], i.e., their velocity error is pressure-dependent, as one can see for an incompressible Stokes model problem $-\nu\Delta\mathbf{u} + \nabla p = \mathbf{f}, \operatorname{div}\mathbf{u} = 0$ with homogeneous Dirichlet velocity boundary conditions (with $\nu > 0$). Here, the velocity errors for the Taylor–Hood and mini elements read as

$$\|\nabla(\mathbf{u} - \mathbf{u}_h)\|_{L^2(\Omega)} \leq C \inf_{\mathbf{w}_h \in \mathbf{V}_h} \|\nabla(\mathbf{u} - \mathbf{w}_h)\|_{L^2(\Omega)} + \frac{1}{\nu} \inf_{q_h \in Q_h} \|p - q_h\|_{L^2(\Omega)},$$

where $\mathbf{V}_h$ and Q_h denote the discrete trial/test spaces for the velocities and the pressures, and C is a $\mathcal{O}(1)$ constant. This velocity error estimate is sharp and shows some kind of locking phenomenon [23, 27, 33, 15, 34]: for small parameters $\nu \ll 1$ the velocity error can become really large. The issue is well-known in the literature, it shows up in real-world situations [10, 18, 29, 23] and it is sometimes called *poor mass conservation* [17], since for H^1-conforming mixed methods such large velocity errors are accompanied by large divergence errors.

Recently, it was shown for several mixed finite element methods like the non-conforming Crouzeix–Raviart element [27, 6] and the conforming P_2^+-P_1^{disc} element [28] (and also for a finite volume [26] and for some Hybrid Discontinuous Galerkin methods [9]), which all use *discontinuous pressures*, that a modification only in the right hand side of the Stokes discretization is able to reestablish pressure-robustness. This approach leads to a velocity error estimate [27, 28]

$$\|\nabla(\mathbf{u} - \mathbf{u}_h)\|_{L^2(\Omega)} \leq C \inf_{\mathbf{w}_h \in \mathbf{V}_h} \|\nabla(\mathbf{u} - \mathbf{w}_h)\|_{L^2(\Omega)} + C_{\mathrm{cons}} h^{l+1} |\mathbf{u}|_{H^{l+1}(\Omega)},$$

where l denotes the approximation order of the discrete pressure space and C_{cons} denotes an $\mathcal{O}(1)$ constant, arising due to a consistency error in the discrete right hand side. Note that similar pressure-robust velocity error estimates can be achieved also with *divergence-free* mixed methods like [38, 44, 45, 21, 22, 25, 16]. The key idea for the modification of the Stokes right hand side in [27] is that discrete divergence-free velocity test functions are mapped to exact divergence-free ones by some velocity reconstruction operator. Then, irrotational parts (in the sense of the continuous Helmholtz decomposition) in the exterior force $\mathbf{f}$ of the above Stokes model problem are orthogonal in the L^2 vector product to (mapped) discrete-divergence velocity test functions and do not spoil the discrete velocity solution $\mathbf{u}_h$ [27]. Indeed, the so-called *poor mass conservation* arises just due to a lack of L^2 orthogonality between discrete-divergence-free velocity test functions and *arbitrary* gradient fields $\nabla \psi$ [26, 27, 23]. For LBB-stable mixed finite element methods with discontinuous pressures the corresponding velocity reconstruction operators employ $H(\mathrm{div})$-conforming finite element spaces. The velocity reconstruction operator is defined elementwise, and fulfills several consistency properties [28].

At the heart of the present contribution lies the construction of novel velocity reconstruction operators for the Taylor–Hood element family and the mini element, which have continuous discrete pressures, such that a modification of the Stokes right hand side yields a pressure-robust mixed method. A first version of such velocity reconstruction operators has been presented in [24]. Similarly, velocity reconstructions in the spirit of [20] could be probably adapted also. Since the new corresponding mixed methods have the same stiffness matrix like their classical counterparts, the discrete LBB condition is inherited from the original method. Optimal convergence of the new pressure-robust mixed methods is shown. The novel velocity reconstructions require the solution of local discrete problems, which are defined on vertex patches. The reconstructions map H^1-conforming velocity test functions to $H(\mathrm{div})$-conforming ones, which preserve the discrete divergence. Especially, discrete divergence-free velocities are mapped to exact divergence-free ones. The construction uses ideas from flux equilibration for a-posteriori estimates [8, 5]. In order to achieve optimal convergence order for the novel mixed methods, the velocity reconstructions have to fulfill some consistency properties, which are incorporated in the local problems to be solved. For this, bubble projectors [14], averaging operators [35] and properties of the Koszul complex [2] have to be exploited.

1.2. Structure of this paper. After defining some notation in the next subsection, in Section 2 the continuous Stokes problem is introduced and the new pressure-robust mixed finite element methods for its discretizations are presented in a quite abstract manner. The main Theorem 2 summarizes the most important properties of the velocity reconstruction operator $\mathcal{R}_h$, while the proofs of these properties are postponed to Section 4 in case of the Taylor–Hood element family and to Section 5 in case of the mini element. Section 3 presents a common finite element error

analysis for the proposed Taylor–Hood and mini element variants. It is shown that their velocity errors are indeed pressure-robust, and that — quite surprisingly — even pressure-robustness results hold for their pressure errors, when measured in some *discrete* pressure norms. In Section 4, different finite element spaces and finite element tools like bubble projectors [14] and Oswald interpolators are introduced, and local (saddle-point) problems on vertex patches are defined that are fundamental for the definition of the novel velocity reconstruction operators for the Taylor–Hood finite element family. Besides proving the unique solvability of these local problems, the properties of the corresponding reconstruction operators stated in Theorem 2 are proved. Similar to Section 4, in Section 5 velocity reconstruction operators for lowest and higher order mini elements are defined solving local problems on vertex patches, and the properties of Theorem 2 are proved also in these cases. Section 6 presents several numerical examples for the incompressible Stokes equations in 2D and 3D that show that the pressure-robust Taylor–Hood and mini element variants can outperform clearly their classical counterparts in the best case, and are only slightly worse than the classical discretizations in the worst case. Section 7 serves as an Appendix where some properties of the Koszul complex in 3D are demonstrated.

1.3. Preliminaries. We introduce some basic notation and assumptions. In this work we assume an open bounded domain $\Omega \subset \mathbb{R}^d$ with $d = 2, 3$ and a Lipschitz boundary Γ. On Ω we define a partition $\Omega = \bigcup_{i=1}^{N_T} T_i$ into sub-domains called elements T_i which will be triangles and tetrahedrons in two and three dimensions respectively. We shall denote $\mathcal{T}$ as such a partition which fulfills a shape regular assumption, so all elements fulfill $|T| \succcurlyeq \operatorname{diam}(T)^d$. Furthermore we call $\mathcal{T}$ quasi–uniform when all elements are essentially of the same size, i.e., there exists one global h such that $h \approx \operatorname{diam}(T), \forall T \in \mathcal{T}$, see for example [4]. The set of vertices is defined as $\mathcal{V}$ and for each vertex $V \in \mathcal{V}$ we define the vertex patch ω_V and the corresponding triangulation $\mathcal{T}_{\omega_V}$ as

$$\omega_V := \bigcup_{T:V \in T} T \subset \Omega \quad \text{and} \quad \mathcal{T}_{\omega_V} := \{T : V \in T\} \subset \mathcal{T},$$

and define the local mesh size $h_V := \max\{\operatorname{diam}(T) : T \in \mathcal{T}_{\omega_V}\}$. We define the polynomial spaces of order m on Ω as $\Pi^m(\Omega)$ and on the triangulation as

$$(1.1) \qquad \Pi^m(\mathcal{T}) := \{q_h : q_h|_T \in \Pi^m(T) \ \forall T \in \mathcal{T}\} = \prod_{T \in \mathcal{T}} \Pi^m(T),$$

and similar for ω_V and $\mathcal{T}_{\omega_V}$. Furthermore we define the spaces

$$L_0^2(\Omega) := \{q \in L^2(\Omega) : \int_\Omega q \ \mathrm{d}x = 0\} =: Q,$$
$$H_0^1(\Omega) := \{u \in H^1(\Omega) : \operatorname{tr} u = 0 \text{ on } \partial\Omega\},$$
$$H_0(\operatorname{div}, \Omega) := \{\boldsymbol{\sigma} \in H(\operatorname{div}, \Omega) : \operatorname{tr}_{\boldsymbol{n}} \sigma = 0 \text{ on } \partial\Omega\},$$
$$\mathbf{V} := [H_0^1(\Omega)]^d,$$
$$\mathbf{V}^0 := \{\mathbf{v} \in \mathbf{V} : \operatorname{div} \mathbf{v} = 0\}.$$

where tr and $\operatorname{tr}_{\boldsymbol{n}}$ denote the trace operators for $H^1(\Omega)$ and $H(\operatorname{div}, \Omega)$. We also define the L^2 projector on polynomials of order m as $\mathcal{P}_\Omega^m$, and the Oswald interpolator $\mathcal{S} : \Pi^m(\mathcal{T}) \to \Pi^m(\mathcal{T}) \cap C^0(\Omega)$ (see [35] or the averaging operator in [12]) that maps discontinuous polynomials to continuous ones. Depending on the dimension we define

4

the Koszul operator (see [2]) for $d = 2$ with $\vec{x} = (x, y)$ and for $d = 3$ with $\vec{x} = (x, y, z)$ as

$$\kappa_{\vec{x}} : L^2(\Omega) \to [L^2(\Omega)]^2 \qquad\qquad \kappa_{\vec{x}} : [L^2(\Omega)]^3 \to [L^2(\Omega)]^3$$

$$\kappa_{\vec{x}}(a) := \begin{pmatrix} -y \\ x \end{pmatrix} a \qquad\qquad \kappa_{\vec{x}}(a) := \vec{x} \times a.$$

Furthermore we define the *Curl* operator for $d = 2$

$$\mathrm{Curl} : \Pi^m(\Omega) \to [\Pi^m(\Omega)]^2$$

$$\mathrm{Curl}\,(u) := (-\partial_y u, \partial_x u)^t.$$

In a similar way all the above introduced spaces and operators can be defines on ω_V. In this work we use $a \preccurlyeq b$ when there exists a constant c independent of a, b, m, h such that $a \leq cb$

2. Continuous and discrete Stokes problems and the velocity reconstruction operator.

The incompressible Stokes problem for a right hand side forcing $\mathbf{f} \in [L^2(\Omega)]^d$ is given in weak formulation by [19]: search for $(\mathbf{u}, p) \in \mathbf{V} \times Q$ such that for all $(\mathbf{v}, q) \in \mathbf{V} \times Q$ holds

$$\begin{aligned} a(\mathbf{u}, \mathbf{v}) + b(\mathbf{v}, p) &= l(\mathbf{v}), \\ b(\mathbf{u}, q) &= 0, \end{aligned} \tag{2.1}$$

where the bilinear forms $a : \mathbf{V} \times \mathbf{V} \to \mathbb{R}$ and $b : \mathbf{V} \times Q \to \mathbb{R}$ and the linear form $l : [L^2(\Omega)]^d \to \mathbb{R}$ are defined by

$$\begin{aligned} a(\mathbf{u}, \mathbf{v}) &= \int_\Omega \nu \nabla \mathbf{u} : \nabla \mathbf{v} \,\mathrm{d}x, \\ b(\mathbf{v}, q) &= \int_\Omega q \,\mathrm{div}\,\mathbf{v} \,\mathrm{d}x, \\ l(\mathbf{v}) &= \int_\Omega \mathbf{f} \cdot \mathbf{v} \,\mathrm{d}x. \end{aligned} \tag{2.2}$$

Note that for the continuous Stokes problem holds the LBB condition

$$\inf_{q \in Q} \sup_{\mathbf{v} \in \mathbf{V}} \frac{b(\mathbf{v}, q)}{\|q\|_{L^2(\Omega)} \|\nabla \mathbf{v}\|_{L^2(\Omega)}} \geq \beta > 0, \tag{2.3}$$

where β denotes the LBB constant.

For the discretization of the continuous Stokes problem (2.1) by inf-sup stable mixed finite element methods [19, 4] we introduce conforming finite element spaces for the velocity $\mathbf{V}_h \subset \mathbf{V}$ and the pressure $Q_h \subset Q$. We assume that for the pair $\mathbf{V}_h \times Q_h$ of discrete spaces holds a discrete LBB condition

$$\inf_{q_h \in Q_h} \sup_{\mathbf{v}_h \in \mathbf{V}_h} \frac{b(\mathbf{v}_h, q_h)}{\|q_h\|_{L^2(\Omega)} \|\nabla \mathbf{v}_h\|_{L^2(\Omega)}} \geq \beta_h > 0. \tag{2.4}$$

We remind the reader that the discrete LBB condition implies the existence of a Fortin interpolator $I_F : \mathbf{V} \to \mathbf{V}_h$ such that for all $\mathbf{v} \in \mathbf{V}$ and for all $q_h \in Q_h$ holds

$$b(I_F \mathbf{v}, q_h) = b(\mathbf{v}, q_h) \qquad \text{and} \qquad \|\nabla I_F \mathbf{v}\|_{L^2(\Omega)} \leq C_F \|\nabla \mathbf{v}\|_{L^2(\Omega)}, \tag{2.5}$$

where C_F denotes the stability constant of the Fortin interpolator [19, 4]. Introducing the space of discrete divergence-free velocity functions

$$(2.6) \qquad \mathbf{V}_h^0 := \{\mathbf{v}_h \in \mathbf{V}_h : b(\mathbf{v}_h, q_h) = 0 \text{ for all } q_h \in Q_h\},$$

the following lemma is a classical result by the theory of mixed finite element methods [19, 4].

LEMMA 1. *Let the finite element spaces $\mathbf{V}_h$ and Q_h fulfill the discrete LBB condition* (2.4), *then it holds for all $\boldsymbol{v} \in \mathbf{V}^0$*

$$\inf_{\boldsymbol{v}_h \in \mathbf{V}_h^0} \|\nabla \boldsymbol{v} - \nabla \boldsymbol{v}_h\|_{L^2(\Omega)} \le (1 + C_F) \inf_{\boldsymbol{w}_h \in \mathbf{V}_h} \|\nabla \boldsymbol{v} - \nabla \boldsymbol{w}_h\|_{L^2(\Omega)}.$$

In the following we propose a non-standard discretization of the right hand side of the Stokes equations, in order to obtain pressure-robust velocity error estimates. Key is the definition of a velocity reconstruction operator in the spirit of [26, 27] that maps discrete divergence-free velocity test functions to exact divergence-free ones. The novelty of this contribution is that we define such reconstruction operators for mixed finite element methods, which possess only *continuous* discrete pressures. The most prominent examples of such mixed finite element methods are given by the Taylor–Hood element family and the mini element [19, 4]. From now on we focus on the Taylor–Hood element of order $k \ge 2$ so

$$\mathbf{V}_h := [\Pi^k(\mathcal{T})]^d \cap [C^0(\Omega)]^d \quad \text{and} \quad Q_h := \Pi^{k-1}(\mathcal{T}) \cap C^0(\Omega),$$

and give a detailed description for the mini element in Section 5. The velocity reconstruction operators

$$\mathcal{R}_h : \mathbf{V}_h \to \mathbf{V}_h + \boldsymbol{\Sigma}_h$$

with some $H(\mathrm{div})$-conforming finite element space $\boldsymbol{\Sigma}_h$ are defined by solving local problems on vertex patches. A precise definition is given in Section 4. We introduce the discrete space of scalar functions

$$(2.7) \qquad \widetilde{Q}_h := \mathrm{div}(\mathcal{R}_h \mathbf{V}_h),$$

and we assume that it holds $Q_h \subset \widetilde{Q}_h$. The Oswald interpolator is now defined from $\mathcal{S} : \widetilde{Q}_h \to Q_h$ with the property

$$(2.8) \qquad \mathcal{S}|_{Q_h(\Omega)} = \mathrm{id}.$$

For the error estimates of the finite element method to be proposed, we use the following abstract properties of $\mathcal{R}_h$, which are summarized in the following theorem.

THEOREM 2. *For the reconstruction operator $\mathcal{R}_h$ defined by equation* (4.19) *holds*

$$(2.9) \quad i. \quad (\mathrm{div}\, \mathcal{R}_h \boldsymbol{w}_h, \tilde{q}_h)_{L^2(\Omega)} = (\mathrm{div}\, \boldsymbol{w}_h, \mathcal{S}\tilde{q}_h)_{L^2(\Omega)} \quad \forall \tilde{q}_h \in \widetilde{Q}_h,$$

$$(2.10) \quad ii. \quad (\mathrm{div}\, (\boldsymbol{w}_h - \mathcal{R}_h \boldsymbol{w}_h), q_h)_{L^2(\Omega)} = 0 \quad \forall \boldsymbol{w}_h \in \mathbf{V}_h, \forall q_h \in Q_h,$$

$$(2.11) \quad iii. \quad (\mathrm{div}\, \boldsymbol{w}_h, q_h)_{L^2(\Omega)} = 0 \; \forall q_h \in Q_h \Rightarrow (\mathrm{div}\, \mathcal{R}_h \boldsymbol{w}_h, \tilde{q}_h)_{L^2(\Omega)} = 0 \; \forall \tilde{q}_h \in \widetilde{Q}_h,$$

$$i.e. \quad \mathrm{div}\, \mathcal{R}_h \boldsymbol{w}_h = 0,$$

$$(2.12) \quad iv. \quad (\boldsymbol{g}, \boldsymbol{w}_h - \mathcal{R}_h \boldsymbol{w}_h)_{L^2(\Omega)} \le C_{\mathrm{cons}} \|\|\boldsymbol{g}\|\|_{k-2} \|\nabla \boldsymbol{w}_h\|_{L^2(\Omega)} \text{ for any } \boldsymbol{g} \in [L^2(\Omega)]^d$$

with data oscillation defined by $\|\|\boldsymbol{g}\|\|_m := \left(\sum_{V \in \mathcal{V}} h_V^2 \|\boldsymbol{g} - \mathcal{P}_{\omega_V}^m \boldsymbol{g}\|_{L^2(\omega_V)}^2 \right)^{\frac{1}{2}}$.

Remark 3. The *data oscillation* $\interleave \cdot \interleave_m$ is similar to a estimation used for the analysis of adaptive methods, see for example [43, p. 60]. Note that for $\mathbf{g} \in H^l(\Omega)$ and a quasi–uniform triangulation $\mathcal{T}$ it follows using a scaling argument that

$$\interleave \mathbf{g} \interleave_m \preccurlyeq h^{\min\{m+2,l+1\}} |\mathbf{g}|_{H^l(\Omega)}.$$

The discrete Stokes problem can now be defined by: search for $(\mathbf{u}_h, p_h) \in \mathbf{V}_h \times Q_h$ such that for all $(\mathbf{v}_h, q_h) \in \mathbf{V}_h \times Q_h$ holds

$$
\begin{aligned}
a(\mathbf{u}_h, \mathbf{v}_h) + b(\mathbf{v}_h, p_h) &= l(\mathcal{R}_h \mathbf{v}_h), \\
b(\mathbf{u}_h, q_h) &= 0.
\end{aligned}
$$
(2.13)

Remark 4. The stiffness matrix of the proposed discretization (2.13) is the same as for standard inf-sup stable mixed finite element methods. However, the discretization of the right hand side is non-standard. The main reason for this non-standard discretization is: for the continuous Stokes problem (2.1) it holds that $(\mathbf{u}, \psi)$ is the solution for arbitrary right hand sides of the form $\mathbf{f} = \nabla\psi$ with $\psi \in H^1(\Omega)/\mathbb{R}$, i.e., irrotational forces $\mathbf{f} = \nabla\psi$ lead to a no-flow velocity solution $\mathbf{u} = \mathbf{0}$ [26, 27]. This is due to the L^2 orthogonality $\int_\Omega \nabla\psi \cdot \mathbf{w} \, dx = 0$ for all $\mathbf{w} \in H_0(\mathrm{div}, \Omega)$ with $\mathrm{div}\, \mathbf{w} = 0$. Similarly it holds $\mathbf{u}_h = \mathbf{0}$ for the discretization (2.13), since due to Theorem 2 discrete divergence-free velocity test functions are mapped to divergence-free ones [26, 27].

3. Error estimation for the pressure-robust Stokes discretization. In this section, an a-priori error analysis is performed for the solution of the discrete Stokes problem $(\mathbf{u}_h, p_h)$ in (2.13). The following lemma is needed to estimate the consistency error introduced due to the non-standard discretization of the right hand side in (2.13).

LEMMA 5. *For $\boldsymbol{v} \in \mathbf{V}$ with $\Delta\boldsymbol{v} \in [L^2(\Omega)]^d$ and for all $\boldsymbol{w}_h \in \mathbf{V}_h$ it holds*

$$|(\Delta\boldsymbol{v}, \mathcal{R}_h \boldsymbol{w}_h) + (\nabla\boldsymbol{v}, \nabla\boldsymbol{w}_h)| \le C_{\mathrm{cons}} \interleave \Delta\boldsymbol{v} \interleave_{k-2} \|\nabla\boldsymbol{w}_h\|_{L^2(\Omega)}.$$

Proof. By calculating and applying (2.12), one obtains

$$
\begin{aligned}
(\Delta\mathbf{v}, \mathcal{R}_h \mathbf{w}_h) + (\nabla\mathbf{v}, \nabla\mathbf{w}_h) &= (\Delta\mathbf{v}, \mathcal{R}_h \mathbf{w}_h - \mathbf{w}_h) + (\Delta\mathbf{v}, \mathbf{w}_h) + (\nabla\mathbf{v}, \nabla\mathbf{w}_h) \\
&= (\Delta\mathbf{v}, \mathcal{R}_h \mathbf{w}_h - \mathbf{w}_h) \le C_{\mathrm{cons}} \interleave \Delta\mathbf{v} \interleave_{k-2} \|\nabla\mathbf{w}_h\|_{L^2(\Omega)}. \quad \Box
\end{aligned}
$$

THEOREM 6. *For the discrete solution $(\boldsymbol{u}_h, p_h) \in \mathbf{V}_h \times Q_h$ in (2.13) and the continuous solution $(\boldsymbol{u}, p) \in (\mathbf{V}, Q)$ of (2.1), assuming the regularity $\Delta\boldsymbol{u} \in [L^2(\Omega)]^d$ the following a-priori errors hold*

i. $\quad \|\nabla(\boldsymbol{u} - \boldsymbol{u}_h)\|_{L^2(\Omega)} \le 2(1 + C_F) \inf_{\boldsymbol{w}_h \in \mathbf{V}_h} \|\nabla(\boldsymbol{u} - \boldsymbol{w}_h)\|_{L^2(\Omega)} + C_{\mathrm{cons}} \interleave \Delta\boldsymbol{u} \interleave_{k-2},$

(3.1)

ii. $\quad \|\mathcal{SP}_{\widetilde{Q}_h} p - p_h\|_{L^2(\Omega)} \le \dfrac{\nu}{\beta_h} \left(\|\nabla(\boldsymbol{u} - \boldsymbol{u}_h)\|_{L^2(\Omega)} + C_{\mathrm{cons}} \interleave \Delta\boldsymbol{u} \interleave_{k-2} \right),$

iii. $\quad \|p - p_h\|_{L^2(\Omega)} \le \|p - \mathcal{SP}_{\widetilde{Q}_h} p\|_{L^2(\Omega)}$

$$+ \dfrac{\nu}{\beta_h} \left(\|\nabla(\boldsymbol{u} - \boldsymbol{u}_h)\|_{L^2(\Omega)} + C_{\mathrm{cons}} \interleave \Delta\boldsymbol{u} \interleave_{k-2} \right).$$

Proof. Note that from $\Delta \mathbf{u} \in [L^2(\Omega)]^d$ and $\mathbf{f} \in [L^2]^d(\Omega)$ follows $p \in H^1(\Omega)$. i) For an arbitrary $\mathbf{v}_h \in \mathbf{V}_h^0$ we define $\mathbf{w}_h := \mathbf{u}_h - \mathbf{v}_h \in \mathbf{V}_h^0$.

$$
\begin{aligned}
\nu \left\| \nabla \mathbf{w}_h \right\|_{L^2(\Omega)}^2 &= a(\mathbf{w}_h, \mathbf{w}_h) = a(\mathbf{u}_h, \mathbf{w}_h) - a(\mathbf{v}_h, \mathbf{w}_h) \\
&= (-\nu \Delta \mathbf{u} + \nabla p, \mathcal{R}_h \mathbf{w}_h) - a(\mathbf{v}_h, \mathbf{w}_h) \\
&= a(\mathbf{u} - \mathbf{v}_h, \mathbf{w}_h) - \nu \left((\Delta \mathbf{u}, \mathcal{R}_h \mathbf{w}_h) + (\nabla \mathbf{u}, \nabla \mathbf{w}_h) \right),
\end{aligned}
$$

where it was used that $\operatorname{div} \mathcal{R}_h \mathbf{w}_h = 0$ holds due to (2.11) and that thus ∇p and $\mathcal{R}_h \mathbf{w}_h$ are orthogonal in L^2. Using Lemma 5 and the Cauchy–Schwarz inequality yields

$$
\nu \left\| \nabla \mathbf{w}_h \right\|_{L^2(\Omega)}^2 \leq \nu \left\| \nabla(\mathbf{u} - \mathbf{v}_h) \right\|_{L^2(\Omega)} \left\| \nabla \mathbf{w}_h \right\|_{L^2(\Omega)} + \nu C_{\mathrm{cons}} \|\Delta \mathbf{u}\|_{k-2} \left\| \nabla \mathbf{w}_h \right\|_{L^2(\Omega)}.
$$

Therefore it holds

$$
\left\| \nabla \mathbf{w}_h \right\|_{L^2(\Omega)} \leq \inf_{\mathbf{v}_h \in \mathbf{V}_h^0} \left\| \nabla(\mathbf{u} - \mathbf{v}_h) \right\|_{L^2(\Omega)} + C_{\mathrm{cons}} \|\Delta \mathbf{u}\|_{k-2}.
$$

With the triangle inequality it follows

$$
\left\| \nabla(\mathbf{u} - \mathbf{u}_h) \right\|_{L^2(\Omega)} \leq \left\| \nabla(\mathbf{u} - \mathbf{v}_h) \right\|_{L^2(\Omega)} + \left\| \nabla \mathbf{w}_h \right\|_{L^2(\Omega)}.
$$

Applying Lemma 1 yields the first statement.

ii) For proving the pressure error, one computes for an arbitrary $\mathbf{v}_h \in \mathbf{V}_h$

$$
\begin{aligned}
(\mathcal{SP}_{\widetilde{Q}_h} p - p_h, \operatorname{div} \mathbf{v}_h) &= (\mathcal{SP}_{\widetilde{Q}_h} p, \operatorname{div} \mathbf{v}_h) + (\mathbf{f}, \mathcal{R}_h \mathbf{v}_h) - a(\mathbf{u}_h, \mathbf{v}_h) \\
&= (\mathcal{P}_{\widetilde{Q}_h} p, \operatorname{div} \mathcal{R}_h \mathbf{v}_h) + (\nabla p, \mathcal{R}_h \mathbf{v}_h) - (\nu \Delta \mathbf{u}, \mathcal{R}_h \mathbf{v}_h) - a(\mathbf{u}_h, \mathbf{v}_h) \\
&= -(\nu \Delta \mathbf{u}, \mathcal{R}_h \mathbf{v}_h) - a(\mathbf{u}_h, \mathbf{v}_h) \\
&= -(\nu \Delta \mathbf{u}, \mathcal{R}_h \mathbf{v}_h) - a(\mathbf{u}, \mathbf{v}_h) - a(\mathbf{u}_h - \mathbf{u}, \mathbf{v}_h),
\end{aligned}
$$

where (2.9) was used. Using the discrete LBB condition (2.4), one concludes

$$
\|\mathcal{SP}_{\widetilde{Q}_h} p - p_h\|_{L^2(\Omega)} \leq \frac{\nu}{\beta_h} \left(\left\| \nabla(\mathbf{u} - \mathbf{u}_h) \right\|_{L^2(\Omega)} + C_{\mathrm{cons}} \|\Delta \mathbf{u}\|_{k-2} \right).
$$

iii) The last statement follows by the triangle inequality. □

Remark 7. The statement i) in Theorem 6 shows the pressure-robustness of the a-priori velocity error. Interesting is also statement ii) in Theorem 6. It shows that also the pressure error is pressure-robust in the sense that $p_h = \mathcal{SP}_{\widetilde{Q}_h} p$ up to an error, which is only velocity-dependent. Note that this is completely analogous to pressure-robust mixed methods with discontinuous pressures [28, 30, 6]. There, Q_h and $\widetilde{Q}_h$ coincide and p_h is even the *best approximation* of p in Q_h up to an error, which is also only velocity-dependent.

COROLLARY 8. *Assume a quasi-uniform triangulation $\mathcal{T}$ and a solution $\boldsymbol{u} \in [H^{k+1}(\Omega)]^d$ and $p \in H^k(\Omega)$ of the continuous problem (2.1). Then, the solution $(\boldsymbol{u}_h, p_h)$ of (2.13) satisfies*

$$
\|\boldsymbol{u} - \boldsymbol{u}_h\|_{H^1(\Omega)} \leq \left(2(1 + C_F) + C_{\mathrm{cons}} \right) h^k |\boldsymbol{u}|_{H^{k+1}(\Omega)}, \quad \text{and} \tag{3.2}
$$

$$
\|p - p_h\|_{L^2(\Omega)} \leq \frac{\nu \left(2(1 + C_F) + 2C_{\mathrm{cons}} \right)}{\beta} h^k |\boldsymbol{u}|_{H^{k+1}(\Omega)} + h^k |p|_{H^k(\Omega)}. \tag{3.3}
$$

Proof. Follows by Theorem 3.1 and standard scaling arguments. □

Remark 9. In order to increase the accuracy of the solution one may want to use a local refinement of the mesh $\mathcal{T}$. This is indeed possible with the modified method due to local properties of the *data oscillation*.

COROLLARY 10. *Under the assumptions of Theorem 6, Corollary 8 and the convexity of Ω it holds*

$$\|\boldsymbol{u} - \boldsymbol{u}_h\|_{L^2(\Omega)} \preccurlyeq h^{k+1} |\boldsymbol{u}|_{H^{k+1}(\Omega)}.$$

Proof. The proof follows by an Aubin–Nitsche argument [4, 3, 32]. For an arbitrary $\mathbf{g} \in [L^2(\Omega)]^d$ one employs a dual Stokes problem with a solution $\mathbf{u_g} \in \mathbf{V}^0 \cap [H^2(\Omega)]^d$. Extending the domain of definition of the reconstruction operator $\mathcal{R}_h$ to $\mathbf{V}^0$ one sees at once that it holds $\mathcal{R}_h \mathbf{w} = \mathbf{w}$ for all $\mathbf{w} \in \mathbf{V}^0$. Then, $\mathcal{R}_h \mathbf{u_g} = \mathbf{u_g}$ and the arguments in [28] deliver the desired optimal pressure-robust L^2-estimate. □

4. Construction and analysis of the reconstruction operator.

4.1. Definition of the operators and spaces. In this section we define local problems on each vertex patch ω_V and proof theorem 2. For an arbitrary vertex $V \in \mathcal{V}$ we start by defining the spaces

$$\Sigma_{h,0}(\mathcal{T}_{\omega_V}) := \{\boldsymbol{\sigma}_h \in \mathcal{RT}^{k-1}(\mathcal{T}_{\omega_V}) : \mathrm{tr}_{\boldsymbol{n}}\boldsymbol{\sigma}_h = 0 \text{ on } \partial\omega_V\} \subset H_0(\mathrm{div}, \omega_V)$$
$$\widetilde{Q}_h(\mathcal{T}_{\omega_V}) := \Pi^{k-1}(\mathcal{T}_{\omega_V}) \subset L^2(\omega_V) \qquad \widetilde{Q}_h^0(\mathcal{T}_{\omega_V}) := \widetilde{Q}_h(\mathcal{T}_{\omega_V}) \cap L_0^2(\omega_V),$$

where $\mathcal{RT}^{k-1}$ is the Raviart-Thomas space of order $k-1$ see [4] and [36] , and for $k \geq 3$ using the Koszul operator also

$$W_h(\omega_V) := \kappa_{\vec{x}-V}(\Pi^{k-3}(\omega_V)) \subset \Lambda_V := \kappa_{\vec{x}-V}(L^2(\omega_V)) \quad \text{for} \quad d = 2$$
$$W_h(\omega_V) := \kappa_{\vec{x}-V}([\Pi^{k-3}(\omega_V)]^3) \subset \Lambda_V := \kappa_{\vec{x}-V}([L^2(\omega_V)]^3) \quad \text{for} \quad d = 3.$$

Note that $\widetilde{Q}_h$ consists of element-wise polynomials and $\Pi^{k-3}(\omega_V)$ are polynomials on the patch. Furthermore we have the property

(4.1) $$\mathrm{div}\,\Sigma_{h,0}(\mathcal{T}_{\omega_V}) = \widetilde{Q}_h^0(\mathcal{T}_{\omega_V}).$$

We continue with the definition of the bilinearform $\mathcal{B} : (H_0(\mathrm{div}, \omega_V) \times L_0^2(\omega_V) \times \Lambda_V) \times (H_0(\mathrm{div}, \omega_V) \times L_0^2(\omega_V) \times \Lambda_V) \to \mathbb{R}$ by

$$\mathcal{B}((\boldsymbol{\sigma}, \phi, \boldsymbol{\lambda}), (\boldsymbol{\tau}, \psi, \boldsymbol{\mu})) :=$$
$$\int_{\omega_V} \boldsymbol{\sigma} \cdot \boldsymbol{\tau}\,\mathrm{d}x + \int_{\omega_V} \mathrm{div}\,\boldsymbol{\tau}\phi\,\mathrm{d}x + \int_{\omega_V} \boldsymbol{\tau} \cdot \boldsymbol{\lambda}\,\mathrm{d}x + \int_{\omega_V} \mathrm{div}\,\boldsymbol{\sigma}\psi\,\mathrm{d}x + \int_{\omega_V} \boldsymbol{\sigma} \cdot \boldsymbol{\mu}\,\mathrm{d}x.$$

Now let T be an arbitrary element $T \in \mathcal{T}$, and $\mathcal{V}_T$ be the set of vertices of T with $N_T := |\mathcal{V}_T|$. Let $\{\phi_j\}_{j=1}^{N_T}$ be the local (Lagrangian) basis on T for the interpolation points $\{x_j\}_{j=1}^{N_T}$ and $\{q_j\}_{j=1}^{N_T}$ be the coefficients of an arbitrary $q \in \Pi^{k-1}(T)$, so

$$\phi_j(x_l) = \delta_{jl} \quad \forall j, l = 1, \dots, N_T \qquad \text{and} \qquad q(x) = \sum_{j=1}^{N_T} q_j \phi_j(x).$$
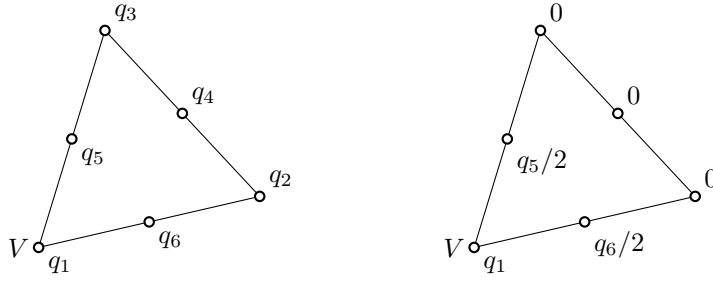
Fig. 1: Visualisation of the nodal coefficients $q_1, \ldots, q_6$ of a quadratic polynomial $q \in \Pi^2(T)$ (left) and the coefficients of its bubble projector $\mathcal{P}^{\mathcal{B}}_{T,V} q$ (right) on a triangle T with respect to the vertex V.

Then we define for each $V \in \mathcal{V}_T$ an operator $\mathcal{P}^{\mathcal{B}}_{T,V} : \Pi^{k-1}(T) \to \Pi^{k-1}(T)$ by setting the coefficients as

$$(4.2) \qquad (\mathcal{P}^{\mathcal{B}}_{T,V} q)_j = q_j \lambda_V(x_j),$$

where λ_V is the barycentric coordinate function of the vertex V. Figure 1 visualizes the change in the coefficients for a quadratic polynomial in two dimensions. It holds

$$(4.3) \qquad \mathrm{tr}\mathcal{P}^{\mathcal{B}}_{T,V} q = 0 \;\; \text{on} \;\; F_{op} \qquad \text{and} \qquad \sum_{V \in \mathcal{V}_T} \mathcal{P}^{\mathcal{B}}_{T,V} q = q,$$

where F_{op} is the opposite edge of V for $d = 2$ and the opposite face for $d = 3$. Using a trivial extension by 0 on $\Omega \setminus T$, we can expand the range of $\mathcal{P}^{\mathcal{B}}_{T,V}$ on $\widetilde{Q}_h(\mathcal{T})$. By that we define for every vertex V the *bubble projector* $\mathcal{P}^{\mathcal{B}}_V : \widetilde{Q}_h(\mathcal{T}) \to \widetilde{Q}_h(\mathcal{T})$ as

$$(4.4) \qquad \mathcal{P}^{\mathcal{B}}_V \tilde{q}_h := \sum_{T \in \mathcal{T}_{\omega_V}} \mathcal{P}^{\mathcal{B}}_{T,V} \tilde{q}_h \quad \forall \tilde{q}_h \in \widetilde{Q}_h(\mathcal{T}),$$

with the property

$$(4.5) \qquad \mathrm{tr}\mathcal{P}^{\mathcal{B}}_V \tilde{q}_h = 0 \quad \text{on} \quad \partial\omega_V.$$
$$(4.6) \qquad \mathcal{P}^{\mathcal{B}}_V \tilde{q}_h = 0 \quad \text{on} \quad \Omega \setminus \omega_V.$$

In Figure 2 an example of a projected arbitrary $\tilde{q}_h \in \widetilde{Q}_h$ is given.

Remark 11. More complicated, but polynomial-robust *bubble projectors* are given in [41] and [14]. If this robustness is an issue, these operators could be used instead of $\mathcal{P}^{\mathcal{B}}_V$.

4.2. Definition of the local problem. On the vertex patch, we define the problem: For a given function $\mathrm{div}\, \boldsymbol{w}_h \in \widetilde{Q}_h(\mathcal{T}_{\omega_V})$ find $(\boldsymbol{\sigma}^V_h, \phi_h, \boldsymbol{\lambda}_h) \in (\Sigma_{h,0}(\mathcal{T}_{\omega_V}) \times \widetilde{Q}^0_h(\mathcal{T}_{\omega_V}) \times W_h(\omega_V))$ so that

$$(4.7) \qquad \mathcal{B}((\boldsymbol{\sigma}^V_h, \phi_h, \boldsymbol{\lambda}_h), (\boldsymbol{\tau}_h, \psi_h, \boldsymbol{\mu}_h)) = \left(\mathrm{div}\, \boldsymbol{w}_h, \mathcal{P}^{\mathcal{B}}_V (\psi_h - \mathcal{S}\psi_h)\right)_{L^2(\omega_V)}$$

$$\forall (\boldsymbol{\tau}_h, \psi_h, \boldsymbol{\mu}_h) \in \Sigma_{h,0}(\mathcal{T}_{\omega_V}) \times \widetilde{Q}^0_h(\mathcal{T}_{\omega_V}) \times W_h(\omega_V).$$
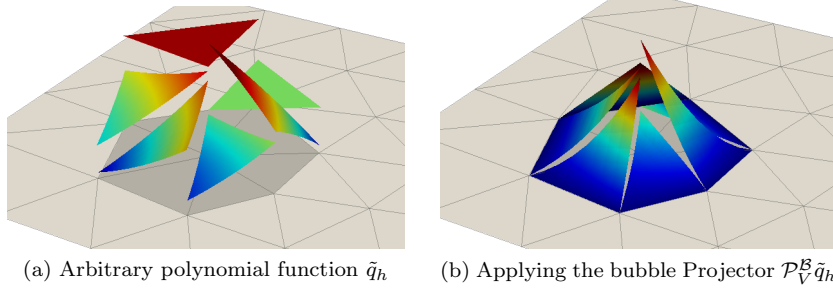
(a) Arbitrary polynomial function $\tilde{q}_h$ (b) Applying the bubble Projector $\mathcal{P}_V^{\mathcal{B}}\tilde{q}_h$

Fig. 2: An example for the bubble projector on ω_V (dark gray)

THEOREM 12. *Equation 4.7 has a unique solution $(\boldsymbol{\sigma}_h^V, \phi_h, \boldsymbol{\lambda}_h)$ satisfying*

(4.8)   i. $\left\|\boldsymbol{\sigma}_h^V\right\|_{L^2(\omega_V)} \preccurlyeq h_V \left\|\mathrm{div}\,\boldsymbol{w}_h\right\|_{L^2(\omega_V)},$

(4.9)   ii. $\left(\mathrm{div}\,\boldsymbol{\sigma}_h^V, \tilde{q}_h\right)_{L^2(\Omega)} = \left(\mathrm{div}\,\boldsymbol{w}_h, \mathcal{P}_V^{\mathcal{B}}\left(\tilde{q}_h - \mathcal{S}\tilde{q}_h\right)\right)_{L^2(\omega_V)} \quad \forall \tilde{q}_h \in \widetilde{Q}_h(\mathcal{T})$

       where $\boldsymbol{\sigma}_h^V$ was trivially extended by 0 on Ω,

    iii.   *and the solution is $L^2(\omega_V)$-orthogonal to polynomials of order $k-2$, i.e.*

(4.10) $\left(\boldsymbol{\sigma}_h^V, \xi\right)_{L^2(\omega_V)} = 0 \quad \forall \xi \in [\Pi^{k-2}(\omega_V)]^d.$

Proof of existence, uniqueness and i. We start with the considered norms

$$\|\boldsymbol{\tau}_h\|_{\Sigma_{h,0}(\mathcal{T}_{\omega_V})} := \|\boldsymbol{\tau}_h\|_{L^2(\omega_V)} + h_V \|\mathrm{div}\,\boldsymbol{\tau}_h\|_{L^2(\omega_V)},$$

$$\|\psi_h\|_{\widetilde{Q}_h(\mathcal{T}_{\omega_V})} := \frac{1}{h_V}\|\psi_h\|_{L^2(\omega_V)},$$

$$\|\boldsymbol{\mu}_h\|_{W_h(\omega_V)} := \|\boldsymbol{\mu}_h\|_{L^2(\omega_V)}.$$

In this part of the proof we use $\Sigma_{h,0}$ as symbol for $\Sigma_{h,0}(\mathcal{T}_{\omega_V})$ and similar for $\widetilde{Q}_h(\mathcal{T}_{\omega_V})$ and $W_h(\mathcal{T}_{\omega_V})$. Next we define the bilinearforms

$$a_\sigma(\boldsymbol{\sigma}_h, \boldsymbol{\tau}_h) := \int_{\omega_V} \boldsymbol{\sigma}_h \cdot \boldsymbol{\tau}_h \,\mathrm{d}x \qquad \forall (\boldsymbol{\sigma}_h, \boldsymbol{\tau}_h) \in \Sigma_{h,0} \times \Sigma_{h,0},$$

$$b_1(\boldsymbol{\sigma}_h, \psi_h) := \int_{\omega_V} \mathrm{div}\,\boldsymbol{\sigma}_h \psi_h \,\mathrm{d}x \qquad \forall (\boldsymbol{\sigma}_h, \psi_h) \in \Sigma_{h,0} \times \widetilde{Q}_h,$$

$$b_2(\boldsymbol{\sigma}_h, \boldsymbol{\mu}_h) := \int_{\omega_V} \boldsymbol{\sigma}_h \cdot \boldsymbol{\mu}_h \,\mathrm{d}x \qquad \forall (\boldsymbol{\sigma}_h, \boldsymbol{\mu}_h) \in \Sigma_{h,0} \times W_h.$$

Using the Cauchy Schwarz inequality we see that a_σ, b_1 and b_2 are all continuous

$$a_\sigma(\boldsymbol{\sigma}_h, \boldsymbol{\tau}_h) \preccurlyeq \|\boldsymbol{\sigma}_h\|_{L^2(\omega_V)}\|\boldsymbol{\tau}_h\|_{L^2(\omega_V)} \preccurlyeq \|\boldsymbol{\sigma}_h\|_{\Sigma_{h,0}}\|\boldsymbol{\tau}_h\|_{\Sigma_{h,0}}$$

$$b_1(\boldsymbol{\sigma}_h, \psi_h) \preccurlyeq \|\mathrm{div}\,\boldsymbol{\sigma}_h\|_{L^2(\omega_V)}\|\psi_h\|_{L^2(\omega_V)} \preccurlyeq \|\boldsymbol{\sigma}_h\|_{\Sigma_{h,0}}\|\psi_h\|_{\widetilde{Q}_h}$$

$$b_2(\boldsymbol{\sigma}_h, \boldsymbol{\mu}_h) \preccurlyeq \|\boldsymbol{\sigma}_h\|_{L^2(\omega_V)}\|\boldsymbol{\mu}_h\|_{L^2(\omega_V)} = \|\boldsymbol{\sigma}_h\|_{W_h}\|\boldsymbol{\mu}_h\|_{W_h}.$$

As

$$\mathcal{B}((\boldsymbol{\sigma}_h^V, \phi_h, \boldsymbol{\lambda}_h),(\boldsymbol{\tau}_h, \psi_h, \boldsymbol{\mu}_h)) =$$
$$a_\sigma(\boldsymbol{\sigma}_h, \boldsymbol{\tau}_h) + b_1(\boldsymbol{\sigma}_h, \psi_h) + b_2(\boldsymbol{\sigma}_h, \boldsymbol{\mu}_h) + b_1(\boldsymbol{\tau}_h, \phi_h) + b_2(\boldsymbol{\tau}_h, \boldsymbol{\lambda}_h),$$

we show the existence and uniqueness of the saddle point problem (4.7) as in chapter 4 in [4], so it remains to show the ellipticity of $a_\sigma(\cdot, \cdot)$, i.e.

$$(4.11) \qquad a_\sigma(\boldsymbol{\sigma}_h, \boldsymbol{\sigma}_h) \succcurlyeq \|\boldsymbol{\sigma}_h\|_{\Sigma_{h,0}}^2 \quad \forall \boldsymbol{\sigma}_h \in \Sigma_{h,0}^0$$

on the kernel

$$\Sigma_{h,0}^0 := \{\boldsymbol{\sigma}_h \in \Sigma_{h,0} : b_1(\boldsymbol{\sigma}_h, \psi_h) + b_2(\boldsymbol{\sigma}_h, \boldsymbol{\mu}_h) = 0 \; \forall (\psi_h, \boldsymbol{\mu}_h) \in \widetilde{Q}_h^0 \times W_h\},$$

and the LBB condition with some $\beta_\sigma > 0$ such that, for all $(\psi_h, \boldsymbol{\mu}_h) \in \widetilde{Q}_h^0 \times W_h$,

$$(4.12) \qquad \sup_{\boldsymbol{\sigma}_h \in \Sigma_{h,0}} \frac{b_1(\boldsymbol{\sigma}_h, \psi_h) + b_2(\boldsymbol{\sigma}_h, \boldsymbol{\mu}_h)}{\|\boldsymbol{\sigma}_h\|_{\Sigma_{h,0}}} \succcurlyeq \beta_\sigma (\|\psi_h\|_{\widetilde{Q}_h} + \|\boldsymbol{\mu}_h\|_{W_h}).$$

For a function $\boldsymbol{\sigma}_h$ in the kernel $\Sigma_{h,0}^0$ it holds in particular

$$b_1(\boldsymbol{\sigma}_h, \psi_h) = 0 \quad \forall \psi_h \in \widetilde{Q}_h^0,$$

and hence div $\boldsymbol{\sigma}_h = 0$, thus

$$\|\boldsymbol{\sigma}_h\|_{L^2(\omega_V)} = \|\boldsymbol{\sigma}_h\|_{\Sigma_{h,0}} \quad \forall \boldsymbol{\sigma}_h \in \Sigma_{h,0}^0.$$

This implies (4.11). To show (4.12) we will proceed in three steps. First we show the LBB condition for the bilinearform $b_1(\cdot, \cdot)$ and then for $b_2(\cdot, \cdot)$ by choosing proper candidates that do not destroy the first condition, and finally combine the two estimates. For $b_1(\cdot, \cdot)$ we first show the LBB condition on the reference patch $\widehat{\omega_V}$ and then on ω_V. It should be mentioned that there exist different reference patches due to the number of elements that belong to a vertex, but for each triangulation $\mathcal{T}$ there exist a finite number of reference patches. We use the standard Raviart-Thomas interpolator $I_{\mathcal{RT}}$ of order $k-1$ (see [4], or [11]) that provides

$$b_1(I_{\mathcal{RT}}\boldsymbol{\sigma}, \psi_h) = b_1(\boldsymbol{\sigma}, \psi_h) \quad \forall \psi_h \in \widetilde{Q}_h(\widehat{\omega_V}) \quad \forall \boldsymbol{\sigma} \in H(\mathrm{div}, \widehat{\omega_V})$$

and

$$\|I_{\mathcal{RT}}\boldsymbol{\sigma}\|_{H(\mathrm{div}, \widehat{\omega_V})} \preccurlyeq \|\boldsymbol{\sigma}\|_{H^1(\widehat{\omega_V})} \quad \forall \boldsymbol{\sigma} \in [H^1(\widehat{\omega_V})]^d.$$

For an arbitrary $\hat{\psi}_h \in \widetilde{Q}_h^0(\widehat{\omega_V})$ we have

$$\sup_{\hat{\boldsymbol{\sigma}}_h \in \Sigma_{h,0}(\widehat{\omega_V})} \frac{b_1(\hat{\boldsymbol{\sigma}}_h, \hat{\psi}_h)}{\|\hat{\boldsymbol{\sigma}}_h\|_{H(\mathrm{div}, \widehat{\omega_V})}} \succcurlyeq \sup_{\hat{\boldsymbol{\sigma}} \in [H_0^1(\widehat{\omega_V})]^d} \frac{b_1(I_{\mathcal{RT}}\hat{\boldsymbol{\sigma}}, \hat{\psi}_h)}{\|I_{\mathcal{RT}}\hat{\boldsymbol{\sigma}}\|_{H(\mathrm{div}, \widehat{\omega_V})}}$$

$$\succcurlyeq \sup_{\hat{\boldsymbol{\sigma}} \in [H_0^1(\widehat{\omega_V})]^d} \frac{b_1(\hat{\boldsymbol{\sigma}}, \hat{\psi}_h)}{\|\hat{\boldsymbol{\sigma}}\|_{H^1(\widehat{\omega_V})}}.$$

Next we use the continuous Stokes LBB condition (2.3) to get

$$(4.13) \qquad \sup_{\hat{\boldsymbol{\sigma}}_h \in \Sigma_{h,0}(\widehat{\omega_V})} \frac{b_1(\hat{\boldsymbol{\sigma}}_h, \hat{\psi}_h)}{\|\hat{\boldsymbol{\sigma}}_h\|_{H(\mathrm{div}, \widehat{\omega_V})}} \geq \beta_1 \|\hat{\psi}_h\|_{L^2(\widehat{\omega_V})},$$

with $\beta_1 > 0$ that depends only of the shape and size of the triangles on the reference patch. To show the condition on ω_V we recall the definition of the Piola transformation. Let $F : \hat{T} \to T$ be the mapping of the reference triangle to an arbitrary element T. Then the Piola transformation is defined as

$$\mathcal{P}(\hat{\boldsymbol{\sigma}}) := \frac{1}{\det F'} F' \hat{\boldsymbol{\sigma}} \quad \forall \hat{\boldsymbol{\sigma}} \in [L^2(\hat{T})]^d.$$

For an arbitrary ψ_h we now choose $\hat{\psi}_h = \psi_h$, and define $\boldsymbol{\sigma}_h^1 := \mathcal{P}(\hat{\boldsymbol{\sigma}}_h)$ for $\hat{\boldsymbol{\sigma}}_h$ that delivers the supremum of Equation (4.13). Standard scaling arguments yield

(4.14)

$$\frac{b_1(\boldsymbol{\sigma}_h^1, \psi_h)}{\|\boldsymbol{\sigma}_h^1\|_{\Sigma_{h,0}}} = \frac{\int_{\omega_V} \operatorname{div} \boldsymbol{\sigma}_h^1 \psi_h \, \mathrm{d}x}{\|\boldsymbol{\sigma}_h^1\|_{L^2(\omega_V)} + h_V \|\operatorname{div} \boldsymbol{\sigma}_h^1\|_{L^2(\omega_V)}} \succcurlyeq \frac{h_V^{(d-2)/2} \int_{\widehat{\omega_V}} \operatorname{div} \hat{\boldsymbol{\sigma}}_h \hat{\psi}_h \, \mathrm{d}x}{\|\hat{\boldsymbol{\sigma}}_h\|_{L^2(\widehat{\omega_V})} + \|\operatorname{div} \hat{\boldsymbol{\sigma}}_h\|_{L^2(\widehat{\omega_V})}}$$

$$\geq h_V^{(d-2)/2} \beta_1 \|\hat{\psi}_h\|_{L^2(\widehat{\omega_V})} = \beta_1 \frac{1}{h_V} \|\psi_h\|_{L^2(\omega_V)} = \beta_1 \|\psi_h\|_{\widetilde{Q}_h}.$$

We continue with the LBB condition for $b_2(\cdot, \cdot)$. We start with the case $d = 3$. Choose an arbitrary $\boldsymbol{\mu}_h = \kappa_{\vec{x}-V}(\boldsymbol{\xi}_h) \in W_h$ with $\boldsymbol{\xi}_h \in [\Pi^{k-3}(\omega_V)]^3$. Furthermore, due to theorem 20, we can assume that $\operatorname{div} \boldsymbol{\xi}_h = 0$. Now we define

$$\boldsymbol{\sigma}_h^2 := -\operatorname{curl}(\lambda_V \boldsymbol{\xi}_h)$$

where λ_V is the hat function of the vertex V. Note that we have

(4.15)
$$b_1(\boldsymbol{\sigma}_h^2, \psi_h) = 0.$$

Using integration by parts we get

$$b_2(\boldsymbol{\sigma}_h^2, \boldsymbol{\mu}_h) = -\int_{\omega_V} \operatorname{curl}(\lambda_V \boldsymbol{\xi}_h) \cdot \kappa_{\vec{x}-V}(\boldsymbol{\xi}_h) \, \mathrm{d}x$$

$$= -\int_{\omega_V} (\lambda_V \boldsymbol{\xi}_h) \cdot \operatorname{curl}((\vec{x} - V) \times \boldsymbol{\xi}_h) \, \mathrm{d}x.$$

Using basic vector calculus leads to

$$\operatorname{curl}((\vec{x} - V) \times \boldsymbol{\xi}_h) = (\vec{x} - V) \underbrace{\operatorname{div} \boldsymbol{\xi}_h}_{=0} + \underbrace{\nabla(\vec{x} - V)}_{I} \boldsymbol{\xi}_h - \boldsymbol{\xi}_h \underbrace{\operatorname{div}(\vec{x} - V)}_{=3} - \nabla \boldsymbol{\xi}_h(\vec{x} - V)$$

$$= -2\boldsymbol{\xi}_h - \nabla \boldsymbol{\xi}_h(\vec{x} - V)$$

and so

$$b_2(\boldsymbol{\sigma}_h^2, \boldsymbol{\mu}_h) = -\int_{\omega_V} (\lambda_V \boldsymbol{\xi}_h) \cdot (-2\boldsymbol{\xi}_h - \nabla \boldsymbol{\xi}_h(\vec{x} - V)) \, \mathrm{d}x$$

$$= \int_{\omega_V} 2\lambda_V \boldsymbol{\xi}_h^2 \, \mathrm{d}x + \int_{\omega_V} \lambda_V \boldsymbol{\xi}_h \cdot \nabla \boldsymbol{\xi}_h(\vec{x} - V) \, \mathrm{d}x$$

$$= \int_{\omega_V} 2\lambda_V \boldsymbol{\xi}_h^2 \, \mathrm{d}x + \frac{1}{2} \int_{\omega_V} \lambda_V \nabla \boldsymbol{\xi}_h^2 \cdot (\vec{x} - V) \, \mathrm{d}x$$

$$= \int_{\omega_V} 2\lambda_V \boldsymbol{\xi}_h^2 \, \mathrm{d}x - \frac{1}{2} \int_{\omega_V} \boldsymbol{\xi}_h^2 \underbrace{\operatorname{div}((\vec{x} - V)\lambda_V)}_{3\lambda_V + \nabla \lambda_V(\vec{x} - V)} \, \mathrm{d}x$$

$$= \frac{1}{2} \int_{\omega_V} \lambda_V \boldsymbol{\xi}_h^2 \, \mathrm{d}x - \frac{1}{2} \int_{\omega_V} \boldsymbol{\xi}_h^2 \nabla \lambda_V(\vec{x} - V) \, \mathrm{d}x.$$

On any $T \subset \mathcal{T}_{\omega_V}$ the gradient of λ_V is equivalent to the scaled normal vector $\boldsymbol{n}_V$ on the face opposite to V, and one can see that $-\boldsymbol{n}_V \cdot (\vec{x} - V) \leq 0$, what finally leads to

$$(4.16) \qquad b_2(\boldsymbol{\sigma}_h^2, \boldsymbol{\mu}_h) \succcurlyeq \beta_2 \|\boldsymbol{\xi}_h\|_{L^2(\omega_V)}^2 \succcurlyeq \beta_2 \|\boldsymbol{\mu}_h\|_{W_h}^2 .$$

For the case $d = 2$ we proceed similar. For an arbitrary $\boldsymbol{\mu}_h = \kappa_{\vec{x}-V}(\xi_h) \in W_h$ with $\xi_h \in \Pi^{k-3}(\omega_V)$ we define

$$\boldsymbol{\sigma}_h^2 := -\mathrm{Curl}\,(\lambda_V \xi_h)$$

Again it holds property (4.15) and we see

$$b_2(\boldsymbol{\sigma}_h^2, \boldsymbol{\mu}_h) = -\int_{\omega_V} \mathrm{Curl}\,(\lambda_V \xi_h) \cdot \kappa_{\vec{x}-V}(\xi_h)\,\mathrm{d}x$$

$$= -\int_{\omega_V} \nabla(\lambda_V \xi_h) \cdot (\vec{x} - V)\xi_h\,\mathrm{d}x$$

$$= \int_{\omega_V} (\lambda_V \xi_h)\,\mathrm{div}\,((\vec{x} - V)\xi_h)\,\mathrm{d}x$$

$$= \int_{\omega_V} 2\lambda_V \xi_h^2 + \frac{1}{2}\int_{\omega_V} \lambda_V (\vec{x} - V)\nabla \xi_h^2\,\mathrm{d}x.$$

The rest is similar as before. Now we can show (4.12). For an arbitrary $\psi_h \in \widetilde{Q}_h^0$ and $\boldsymbol{\mu}_h \in W_h$ we choose the functions $\boldsymbol{\sigma}_h^1, \boldsymbol{\sigma}_h^2$ that fulfill Equations (4.14) and (4.16) and (4.15). Furthermore we can scale $\boldsymbol{\sigma}_h^1$ and $\boldsymbol{\sigma}_h^2$ so that

$$\left\|\boldsymbol{\sigma}_h^1\right\|_{\Sigma_{h,0}} = \|\psi_h\|_{\widetilde{Q}_h} \quad \text{and} \quad \left\|\boldsymbol{\sigma}_h^2\right\|_{\Sigma_{h,0}} = \|\boldsymbol{\mu}_h\|_{W_h} .$$

For $\alpha = \frac{1}{\beta_1 \beta_2}$ we define then $\boldsymbol{\sigma}_h = \boldsymbol{\sigma}_h^1 + \alpha \boldsymbol{\sigma}_h^2$ and get

$$b_1(\boldsymbol{\sigma}_h, \psi_h) + b_2(\boldsymbol{\sigma}_h, \boldsymbol{\mu}_h) = b_1(\boldsymbol{\sigma}_h^1, \psi_h) + b_2(\boldsymbol{\sigma}_h^1, \boldsymbol{\mu}_h) + \alpha b_2(\boldsymbol{\sigma}_h^2, \boldsymbol{\mu}_h)$$

$$\succcurlyeq \beta_1 \|\psi_h\|_{\widetilde{Q}_h}^2 - \left\|\boldsymbol{\sigma}_h^1\right\|_{\Sigma_{h,0}} \|\boldsymbol{\mu}_h\|_{W_h} + \alpha\beta_2 \|\boldsymbol{\mu}_h\|_{W_h}^2$$

$$\succcurlyeq \beta_1 \|\psi_h\|_{\widetilde{Q}_h}^2 - \|\psi_h\|_{\widetilde{Q}_h} \|\boldsymbol{\mu}_h\|_{W_h} + \alpha\beta_2 \|\boldsymbol{\mu}_h\|_{W_h}^2 .$$

Using Young's inequality we have

$$\|\psi_h\|_{\widetilde{Q}_h} \|\boldsymbol{\mu}_h\|_{W_h} \leq \frac{\beta_1}{2} \|\psi_h\|_{\widetilde{Q}_h}^2 + \frac{1}{2\beta_1} \|\boldsymbol{\mu}_h\|_{W_h}^2 ,$$

and so

$$b_1(\boldsymbol{\sigma}_h, \psi_h) + b_2(\boldsymbol{\sigma}_h, \boldsymbol{\mu}_h) \succcurlyeq \frac{\beta_1}{2} \|\psi_h\|_{\widetilde{Q}_h}^2 + \frac{1}{2\beta_1} \|\boldsymbol{\mu}_h\|_{W_h}^2$$

$$\succcurlyeq \left(\frac{\beta_1}{2} + \frac{1}{2\beta_1}\right) (\|\psi_h\|_{\widetilde{Q}_h} + \|\boldsymbol{\mu}_h\|_{W_h})^2.$$

As $\|\boldsymbol{\sigma}_h\|_{\Sigma_{h,0}} = \left\|\boldsymbol{\sigma}_h^1 + \alpha\boldsymbol{\sigma}_h^2\right\|_{\Sigma_{h,0}} \leq (1 + \alpha)(\|\psi_h\|_{\widetilde{Q}_h} + \|\boldsymbol{\mu}_h\|_{W_h})$ we get

$$\frac{b_1(\boldsymbol{\sigma}_h, \psi_h) + b_2(\boldsymbol{\sigma}_h, \boldsymbol{\mu}_h)}{\|\boldsymbol{\sigma}_h\|_{\Sigma_{h,0}}} \succcurlyeq \beta(\|\psi_h\|_{\widetilde{Q}_h} + \|\boldsymbol{\mu}_h\|_{W_h})$$

14

and thus (4.12) holds with $\beta_\sigma = \frac{\beta_1^2+1}{2\beta_1(1+\alpha)}$. Using the theory of saddle point problems, chapter 4 in [4], Equation (4.7) has a unique and stable solution $\boldsymbol{\sigma}_h^V$ that fulfills

$$(4.17) \qquad \left\|\boldsymbol{\sigma}_h^V\right\|_{L^2(\omega_V)} \preccurlyeq \|\operatorname{div} \boldsymbol{w}_h\|_{\widetilde{Q}_h'} \preccurlyeq h_V \|\operatorname{div} \boldsymbol{w}_h\|_{L^2(\omega_V)},$$

so property (4.8) was shown. $\qquad\qquad\square$

Remark 13. In the first step of the above estimation the constant depends on the operator norms of $\mathcal{P}_V^\mathcal{B}$ und $\mathcal{S}$ which are independent of h. For $\mathcal{S}$ we refer to [35],[12]. For the $\mathcal{P}_V^\mathcal{B}$ using the implementation given by the coefficients (4.2) the estimation is clear as $\lambda_{V_i}(x_j) \in (0,1)$.

Proof of ii. and iii.. Now let $c \in \mathbb{R}$ be a constant on the patch, then the right hand side of Equation (4.7) reads as

$$\int_{\omega_V} \operatorname{div} \boldsymbol{w}_h \underbrace{\mathcal{P}_V^\mathcal{B}(c - \mathcal{S}c)}_{=0} \, \mathrm{d}x = 0,$$

but as also

$$\int_{\omega_V} \operatorname{div} \boldsymbol{\sigma}_h^V c \, \mathrm{d}x = c \int_{\partial\omega_V} \boldsymbol{\sigma}_h^V \cdot n \, \mathrm{d}x = 0,$$

it follows that the solution $\boldsymbol{\sigma}_h^V$ fulfills even

$$\int_{\omega_V} \operatorname{div} \boldsymbol{\sigma}_h^V \psi_h \, \mathrm{d}x = \left(\operatorname{div} \boldsymbol{w}_h, \mathcal{P}_V^\mathcal{B}(\psi_h - \mathcal{S}\psi_h)\right)_{L^2(\omega_V)} \quad \forall \psi_h \in \widetilde{Q}_h(\mathcal{T}_{\omega_V}),$$

in contrast to the restriction on $\widetilde{Q}_h^0(\mathcal{T}_{\omega_V})$. Using a trivial extension by $\mathbf{0}$ on $\Omega \setminus \omega_V$ we get (4.9). To show (4.10) we use a decomposition of the polynomial space of order $k-2$ given by

$$(4.18) \qquad \begin{aligned} [\Pi^{k-2}(\omega_V)]^2 &= \nabla\Pi^{k-1}(\omega_V) \oplus \kappa_{\vec{x}-V}(\Pi^{k-3}(\omega_V)) \\ [\Pi^{k-2}(\omega_V)]^3 &= \nabla\Pi^{k-1}(\omega_V) \oplus \kappa_{\vec{x}-V}([\Pi^{k-3}(\omega_V)]^3), \end{aligned}$$

see [2], Equation (3.11). Note that by the shift invariance of polynomial spaces, the origin of the Koszul operator κ can be set to an arbitrary point V. For an arbitrary $b_h \in \Pi^{k-1}(\omega_V) \subset \widetilde{Q}_h(\mathcal{T}_{\omega_V})$ we get using the properties of the bubble projector (4.5) and the Oswald operator

$$\int_{\omega_V} \boldsymbol{\sigma}_h^V \cdot \nabla b_h \, \mathrm{d}x = -\int_{\omega_V} \operatorname{div} \boldsymbol{\sigma}_h^V b_h \, \mathrm{d}x = -\int_{\omega_V} \operatorname{div} \boldsymbol{w}_h \underbrace{\mathcal{P}_V^\mathcal{B}(b_h - \mathcal{S}b_h)}_{=0} \, \mathrm{d}x = 0.$$

As $\kappa_{\vec{x}-V}([\Pi^{k-3}(\omega_V)]^3) = W_h(\omega_V)$ we already know that the solution $\boldsymbol{\sigma}_h^V$ of (4.7) fulfills

$$b_2(\boldsymbol{\sigma}_h^V, \boldsymbol{\mu}_h) = \int_{\omega_V} \boldsymbol{\sigma}_h^V \cdot \kappa_{\vec{x}-V}(\boldsymbol{\xi}_h) \, \mathrm{d}x = 0$$

and so it follows (4.10). For the case $d = 2$ the argument is the same. $\qquad\square$

4.3. Definition of the reconstruction $\mathcal{R}_h$. Now we can define the reconstruction. For that we define the space

$$\Sigma_h := \mathcal{RT}^{k-1}(\mathcal{T}) \subset H(\operatorname{div}, \Omega).$$

For a given $\boldsymbol{w}_h \in \mathbf{V}_h$ and all $V \in \mathcal{V}$ let $\boldsymbol{\sigma}_h^V$ be the solution of Equation (4.7) on ω_V extended by 0 on $\Omega \setminus \omega_V$. Then we define the reconstruction as

$$(4.19) \qquad \mathcal{R}_h \boldsymbol{w}_h := \boldsymbol{w}_h - \boldsymbol{\sigma}_h \in V_h + \Sigma_h \quad \text{with} \quad \boldsymbol{\sigma}_h := \sum_{V \in \mathcal{V}} \boldsymbol{\sigma}_h^V.$$

Remark 14. Due to the zero normal trace of the solutions $\boldsymbol{\sigma}_h^V$ on the patches ω_V the sum $\boldsymbol{\sigma}_h$ is still normal continuous over facets thus $\boldsymbol{\sigma}_h \in \Sigma_h$.

Proof of theorem 2. For an arbitrary $\tilde{q}_h \in \widetilde{Q}_h$ it holds using (4.9), (4.4) and the properties of the bubble projector (4.3)

$$\begin{aligned}
(\operatorname{div} \mathcal{R}_h \boldsymbol{w}_h, \tilde{q}_h)_{L^2(\Omega)} &= (\operatorname{div} \boldsymbol{w}_h, \tilde{q}_h)_{L^2(\Omega)} - \sum_{V \in \mathcal{V}} (\operatorname{div} \boldsymbol{\sigma}_h^V, \tilde{q}_h)_{L^2(\omega_V)} \\
&= (\operatorname{div} \boldsymbol{w}_h, \tilde{q}_h)_{L^2(\Omega)} - \sum_{V \in \mathcal{V}} (\operatorname{div} \boldsymbol{w}_h, \mathcal{P}_V^{\mathcal{B}}(\tilde{q}_h - \mathcal{S}\tilde{q}_h))_{L^2(\omega_V)} \\
&= (\operatorname{div} \boldsymbol{w}_h, \tilde{q}_h)_{L^2(\Omega)} - (\operatorname{div} \boldsymbol{w}_h, \underbrace{\sum_{V \in \mathcal{V}} \mathcal{P}_V^{\mathcal{B}}(\tilde{q}_h - \mathcal{S}\tilde{q}_h)}_{=I})_{L^2(\Omega)} \\
&= (\operatorname{div} \boldsymbol{w}_h, \tilde{q}_h)_{L^2(\Omega)} - (\operatorname{div} \boldsymbol{w}_h, \tilde{q}_h)_{L^2(\Omega)} + (\operatorname{div} \boldsymbol{w}_h, \mathcal{S}\tilde{q}_h)_{L^2(\Omega)} \\
&= (\operatorname{div} \boldsymbol{w}_h, \mathcal{S}\tilde{q}_h)_{L^2(\Omega)}.
\end{aligned}$$

By that it follows for an arbitrary $q_h \in Q_h$, due $\mathcal{S}q_h = q_h$, that

$$(\operatorname{div}(\boldsymbol{w}_h - \mathcal{R}_h \boldsymbol{w}_h), q_h)_{L^2(\Omega)} = 0,$$

and if $(\operatorname{div} \boldsymbol{w}_h, q_h)_{L^2(\Omega)} = 0 \; \forall q_h \in Q_h$ that

$$(4.20) \qquad (\operatorname{div} \mathcal{R}_h \boldsymbol{w}_h, \tilde{q}_h)_{L^2(\Omega)} = (\operatorname{div} \boldsymbol{w}_h, \underbrace{\mathcal{S}\tilde{q}_h}_{\in Q_h})_{L^2(\Omega)} = 0.$$

Finally, using (4.10) and (4.8) we get

$$\begin{aligned}
(\mathbf{g}, \boldsymbol{w}_h - \mathcal{R}_h \boldsymbol{w}_h)_{L^2(\Omega)} &= \sum_{V \in \mathcal{V}} (\mathbf{g}, \boldsymbol{\sigma}_h^V)_{L^2(\omega_V)} = \sum_{V \in \mathcal{V}} (\mathbf{g} - \mathcal{P}_{\omega_V}^{k-2}\mathbf{g}, \boldsymbol{\sigma}_h^V)_{L^2(\omega_V)} \\
&\preccurlyeq \sum_{V \in \mathcal{V}} \|\mathbf{g} - \mathcal{P}_{\omega_V}^{k-2}\mathbf{g}\|_{L^2(\omega_V)} \|\boldsymbol{\sigma}_h^V\|_{L^2(\omega_V)} \\
&\preccurlyeq \sum_{V \in \mathcal{V}} \|\mathbf{g} - \mathcal{P}_{\omega_V}^{k-2}\mathbf{g}\|_{L^2(\omega_V)} h_V \|\operatorname{div} \boldsymbol{w}_h\|_{L^2(\omega_V)} \\
&\preccurlyeq \|\|\mathbf{g}\|\|_{k-2} \|\nabla \boldsymbol{w}_h\|_{L^2(\Omega)}. \qquad \square
\end{aligned}$$

5. The Reconstruction operator for the mini finite element method.

For the mini finite element method [1] the bubble enriched velocity spaces read

$$\Pi_+^k(T) := \Pi^k(T) \oplus \left\{ \Pi^{k+d}(T) \cap H_0^1(T) \right\}, \quad \text{and}$$

$$\Pi_+^k(\mathcal{T}) := \{ q_h : q_h|_T \in \Pi_+^k(T) \ \forall T \in \mathcal{T} \}.$$

The definition of the mini element now reads as

$$\mathbf{V}_h := [\Pi_+^k(\mathcal{T})]^d \cap [C^0(\Omega)]^d \quad \text{and} \quad Q_h := \Pi^k(\mathcal{T}) \cap C^0(\Omega).$$

As in the Taylor–Hood case we solve small problems on the vertex patch ω_V but slightly change the right hand side and the polynomial orders. For that we define

$$\Sigma_{h,0}(\mathcal{T}_{\omega_V}) := \{ \boldsymbol{\sigma}_h \in \mathcal{RT}^{k+d-1}(\mathcal{T}_{\omega_V}) : \mathrm{tr}_{\boldsymbol{n}} \boldsymbol{\sigma}_h = 0 \text{ on } \partial\omega_V \} \subset H_0(\mathrm{div}, \omega_V)$$

$$\widetilde{Q}_h(\mathcal{T}_{\omega_V}) := \Pi^{k+d-1}(\mathcal{T}_{\omega_V}) \subset L^2(\omega_V) \qquad \widetilde{Q}_h^0(\mathcal{T}_{\omega_V}) := \widetilde{Q}_h(\mathcal{T}_{\omega_V}) \cap L_0^2(\omega_V),$$

and for $k \geq 2$ also

$$W_h(\omega_V) := \kappa_{\vec{x}-V}(\Pi^{k-2}(\omega_V)) \subset \Lambda_V := \kappa_{\vec{x}-V}(L^2(\omega_V)) \quad \text{for} \quad d = 2$$

$$W_h(\omega_V) := \kappa_{\vec{x}-V}([\Pi^{k-2}(\omega_V)]^3) \subset \Lambda_V := \kappa_{\vec{x}-V}([L^2(\omega_V)]^3) \quad \text{for} \quad d = 3.$$

So for a given function $\boldsymbol{w}_h \in \mathbf{V}_h$ we have $\mathrm{div}\, \boldsymbol{w}_h \in \widetilde{Q}_h(\mathcal{T}_{\omega_V})$ and seek $(\boldsymbol{\sigma}_h^V, \phi_h, \boldsymbol{\lambda}_h) \in (\Sigma_{h,0}(\mathcal{T}_{\omega_V}) \times \widetilde{Q}_h^0(\mathcal{T}_{\omega_V}) \times W_h(\omega_V))$ so that

$$(5.1) \qquad \mathcal{B}((\boldsymbol{\sigma}_h^V, \phi_h, \boldsymbol{\lambda}_h), (\boldsymbol{\tau}_h, \psi_h, \boldsymbol{\mu}_h)) = \left(\mathrm{div}\, \boldsymbol{w}_h, \mathcal{P}_V^{\mathcal{B}} \left(\psi_h - \tilde{\mathcal{S}}\psi_h \right) \right)_{L^2(\omega_V)}$$

$$\forall (\boldsymbol{\tau}_h, \psi_h, \boldsymbol{\mu}_h) \in \Sigma_{h,0}(\mathcal{T}_{\omega_V}) \times \widetilde{Q}_h^0(\mathcal{T}_{\omega_V}) \times W_h(\omega_V),$$

where $\tilde{\mathcal{S}} : \widetilde{Q}_h(\mathcal{T}_{\omega_V}) \to Q_h(\mathcal{T}_{\omega_V})$. Note that $\tilde{\mathcal{S}}$ now maps element-wise polynomials of degree $k + d - 1$ to continuous element-wise polynomials of order k.

Remark 15. This new operator $\tilde{\mathcal{S}}$ can be seen as the Oswald operator $\mathcal{S}$ of order k applied to polynomials of higher degree.

PROPOSITION 16. *Equation 5.1 has a unique solution $(\boldsymbol{\sigma}_h^V, \phi_h, \boldsymbol{\lambda}_h)$ satisfying*

i. $\quad \left\| \boldsymbol{\sigma}_h^V \right\|_{L^2(\omega_V)} \preccurlyeq h_V \left\| \mathrm{div}\, \boldsymbol{w}_h \right\|_{L^2(\omega_V)},$

ii. $\quad \left(\mathrm{div}\, \boldsymbol{\sigma}_h^V, \tilde{q}_h \right)_{L^2(\Omega)} = \left(\mathrm{div}\, \boldsymbol{w}_h, \mathcal{P}_V^{\mathcal{B}} \left(\tilde{q}_h - \tilde{\mathcal{S}}\tilde{q}_h \right) \right)_{L^2(\omega_V)} \qquad \forall \tilde{q}_h \in \widetilde{Q}_h(\mathcal{T})$

$\quad$ *where $\boldsymbol{\sigma}_h^V$ was trivially extended by 0 on Ω,*

iii. *and the solution is $L^2(\omega_V)$-orthogonal on polynomials of order $k-1$, i.e.*

$\quad \left(\boldsymbol{\sigma}_h^V, \xi \right)_{L^2(\omega_V)} = 0 \quad \forall \xi \in [\Pi^{k-1}(\omega_V)]^d.$

Proof. The proof uses exactly the same arguments as the proof of theorem 12. □

The reconstruction is defined as in (4.19).

PROPOSITION 17. *For the reconstruction operator $\mathcal{R}_h$ defined by (4.19) holds*

i. $\quad (\mathrm{div}\, \mathcal{R}_h w_h, \tilde{q}_h)_{L^2(\Omega)} = \left(\mathrm{div}\, w_h, \tilde{\mathcal{S}}\tilde{q}_h \right)_{L^2(\Omega)} \qquad \forall \tilde{q}_h \in \widetilde{Q}_h,$

ii. $\quad (\mathrm{div}\,(\boldsymbol{w}_h - \mathcal{R}_h \boldsymbol{w}_h), q_h)_{L^2(\Omega)} = 0 \quad \forall \boldsymbol{w}_h \in \mathbf{V}_h, \forall q_h \in Q_h,$

iii. $\quad (\mathrm{div}\, \boldsymbol{w}_h, q_h)_{L^2(\Omega)} = 0 \ \forall q_h \in Q_h \Rightarrow (\mathrm{div}\, \mathcal{R}_h w_h, \tilde{q}_h)_{L^2(\Omega)} = 0 \quad \forall \tilde{q}_h \in \widetilde{Q}_h,$

$\quad\qquad\qquad\qquad\qquad\qquad\qquad i.e. \quad \mathrm{div}\, \mathcal{R}_h \boldsymbol{w}_h = 0,$

(5.2) $\quad$ iv. $\quad (\boldsymbol{g}, \boldsymbol{w}_h - \mathcal{R}_h \boldsymbol{w}_h)_{L^2(\Omega)} \leq C_{\mathrm{cons}} \|\|\boldsymbol{g}\|\|_{k-1} \|\nabla \boldsymbol{w}_h\|_{L^2(\Omega)}.$

Proof. The proof uses exactly the same arguments as the proof of theorem 2. In Equation (4.20) it is important that the Oswald operator maps to Q_h, which is the reason to replace $\mathcal{S}$ by $\tilde{\mathcal{S}}$ for the mini element. ☐

Remark 18. The modified mini finite element method also fits in the abstract setting of Section 3, but here the consistency error is of order $k+1$ due to (5.2), i.e.

$$\|\nabla(\mathbf{u} - \mathbf{u}_h)\|_{L^2} \leq 2(1 + C_F) \inf_{\mathbf{w}_h \in \mathbf{V}_h} \|\nabla(\mathbf{u} - \mathbf{w}_h)\|_{L^2} + C_{\text{cons}} \|\|\Delta\mathbf{u}\|\|_{k-1}.$$

Hence, also in case of the mini finite element methods, the pressure-dependent term from the classical estimate is replaced by a pressure-independent consistency error of the same order.

6. Numerical examples. In this section we give several numerical examples to validate and confirm the theoretical findings. As computational framework, including the implementation of the reconstruction operator $\mathcal{R}_h$, we used NGSolve (see [40]) and the NGSpy interface. For all numerical examples we use unstructered, shape regular and quasi-uniform triangulations $\mathcal{T}$ generated by Netgen (see [39]).

6.1. 2d example. The first example studies the solution

$$\mathbf{u} := \text{curl}\, \zeta \quad \text{with} \quad \zeta := x^2(x-1)^2 y^2(y-1)^2 \quad \text{and} \quad p := x^7 + y^7 - \frac{1}{4},$$

of the Stokes problem on the unit square $\Omega = (0,1)^2$ with $\nu = 10^{-3}$ and the right hand side $\mathbf{f} := -\nu\Delta\mathbf{u} - \nabla p$.

Tables 1-3 show the L^2 velocity and pressure errors and their estimated order of convergence (eoc) for the modified Taylor–Hood finite element methods of order $k = 2, 3, 4$. All methods show the optimal convergence orders as expected by the theory. Table 4 allows the same conclusions for the modified mini finite element method of lowest order.

To clearly see the consequences of pressure-robustness, Figure 3 shows the L^2 errors for different $\nu = 10^j$ for $j = -8, \ldots, 3$ on three fixed meshes for the classical and the modified Taylor–Hood finite element method of order $k = 2$. There are several observations to make:

- For $\nu \geq 1$ the irrotational part in the right-hand side $\mathbf{f}$ is not larger than the divergence-free part. In this situation both methods deliver similar errors. Due to the additional consistency error, the errors of the modified method are a bit larger than the errors of the classical method.
- For $\nu < 1$ the irrotational part in the right-hand side $\mathbf{f}$ begins to dominate and so does the pressure-dependent term in the a priori error estimate. As predicted by these estimates, the errors of the classical Taylor–Hood finite element method deteriorate and scale with $1/\nu$. The modified Taylor–Hood method, due to its divergence-free test functions in the right-hand side, does not see the irrotational force and the errors are independent of ν.
- The transition point $\nu \approx 1$ where the error becomes pressure-dominated is the same on all three meshes. Hence, mesh refinement cannot heal this behaviour.
- The velocity error of the modified method is independent of ν, since $\mathbf{u}_h$ is exactly the same for every ν by construction of the discretization. The pressure error however increases for large ν in both the unmodified and the modified method. This is consistent with the error estimate (3.1).

For the mini finite element method the observations are almost identical. However, since the pressure space has the same order as the velocity space, the pressure-
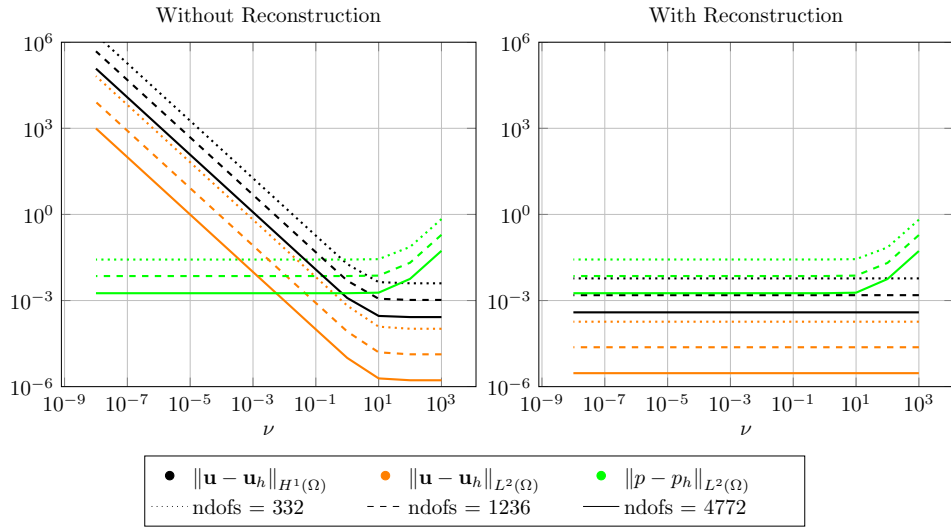
Fig. 3: Errors for the classical (left) and the modified (right) Taylor–Hood finite element method of order $k = 2$ on three fixed meshes and several choices of ν in section 6.1.

#dof	$\|\mathbf{u} - \mathbf{u}_h\|_{H^1}$	eoc	$\|\mathbf{u} - \mathbf{u}_h\|_{L^2}$	eoc	$\|p - p_h\|_{L^2}$	eoc
96	$2.05 \cdot 10^{-2}$		$1.43 \cdot 10^{-3}$		$7.79 \cdot 10^{-2}$	
332	$5.91 \cdot 10^{-3}$	1.794	$1.83 \cdot 10^{-4}$	2.966	$2.69 \cdot 10^{-2}$	1.533
1,236	$1.54 \cdot 10^{-3}$	1.941	$2.36 \cdot 10^{-5}$	2.956	$7.14 \cdot 10^{-3}$	1.913
4,772	$3.88 \cdot 10^{-4}$	1.988	$2.95 \cdot 10^{-6}$	3.000	$1.8 \cdot 10^{-3}$	1.988
18,756	$9.7 \cdot 10^{-5}$	1.999	$3.68 \cdot 10^{-7}$	3.005	$4.51 \cdot 10^{-4}$	1.999

Table 1: Errors for the modified Taylor–Hood finite element method of order $k = 2$ in Section 6.1.

dependent contributions in the a priori error estimates converge faster and can compensate smaller values of ν to some extent.

6.2. 3d example. The second example investigates the velocity and pressure

$$\mathbf{u} := \operatorname{curl}(\zeta, \zeta, \zeta) \quad \text{with} \quad \zeta := x^2(x-1)^2 y^2 (y-1)^2 z^2 (z-1)^2$$

$$p := x^5 + y^5 + z^5 - \frac{1}{2},$$

on the unit cube $\Omega = (0, 1)^3$ for $\nu = 10^{-3}$. Table 5 lists the L^2 errors for the modified Taylor–Hood finite element method of order $k = 2$. Also in this 3D example the convergence rates are optimal.

Remark 19. For the ease of implementation in NGSolve we used Brezzi-Douglas-Marini elements of order k (see [4] and [7]) instead of the Raviart-Thomas elements of order $k - 1$ as basis for the $H(\operatorname{div})$-conforming spaces $\Sigma_h(\mathcal{T})$ and the local spaces $\Sigma_{h,0}(\mathcal{T}_{\omega_V})$. This does not affect the convergence order of the error.

#dof	$\|\mathbf{u} - \mathbf{u}_h\|_{H^1}$	eoc	$\|\mathbf{u} - \mathbf{u}_h\|_{L^2}$	eoc	$\|p - p_h\|_{L^2}$	eoc
212	$3.5 \cdot 10^{-3}$		$1.03 \cdot 10^{-4}$		$1.99 \cdot 10^{-2}$	
772	$4.95 \cdot 10^{-4}$	2.823	$7.02 \cdot 10^{-6}$	3.875	$3.39 \cdot 10^{-3}$	2.554
2,948	$6.07 \cdot 10^{-5}$	3.026	$4.39 \cdot 10^{-7}$	3.999	$4.71 \cdot 10^{-4}$	2.848
11,524	$7.45 \cdot 10^{-6}$	3.028	$2.74 \cdot 10^{-8}$	4.003	$6.08 \cdot 10^{-5}$	2.953
45,572	$9.23 \cdot 10^{-7}$	3.012	$1.71 \cdot 10^{-9}$	3.998	$7.67 \cdot 10^{-6}$	2.986

Table 2: Errors for the modified Taylor–Hood finite element method of order $k = 3$ in Section 6.1.

#dof	$\|\mathbf{u} - \mathbf{u}_h\|_{H^1}$	eoc	$\|\mathbf{u} - \mathbf{u}_h\|_{L^2}$	eoc	$\|p - p_h\|_{L^2}$	eoc
376	$6.04 \cdot 10^{-4}$		$1.46 \cdot 10^{-5}$		$2.95 \cdot 10^{-3}$	
1,404	$3.86 \cdot 10^{-5}$	3.967	$4.73 \cdot 10^{-7}$	4.948	$2.02 \cdot 10^{-4}$	3.868
5,428	$2.34 \cdot 10^{-6}$	4.042	$1.47 \cdot 10^{-8}$	5.011	$1.23 \cdot 10^{-5}$	4.034
21,348	$1.44 \cdot 10^{-7}$	4.028	$4.54 \cdot 10^{-10}$	5.014	$7.6 \cdot 10^{-7}$	4.021
84,676	$8.89 \cdot 10^{-9}$	4.013	$1.41 \cdot 10^{-11}$	5.008	$4.73 \cdot 10^{-8}$	4.007

Table 3: Errors for the modified Taylor–Hood finite element method of order $k = 4$ in Section 6.1.

6.3. Navier–Stokes for a 2D potential flow. This example studies a two-dimensional potential flow for the harmonic potential $\chi := x^5 - 10x^3y^2 + 5xy^4$. Note that χ is the real part of the analytic function z^5 (with $z = x + iy$). We look for the solution of the steady incompressible Navier–Stokes equations $-\nu\Delta\mathbf{u} + (\mathbf{u} \cdot \nabla)\mathbf{u} + \nabla p = \mathbf{0}$, $\text{div}\,\mathbf{u} = 0$ with inhomogeneous Dirichlet boundary conditions for $\nu = 0.1$. The exact solution of the velocity is given by $\mathbf{u} = \nabla\chi$ and $p = 664/63 - 25/2(x^2 + y^2)^4$, modelling the collision of five jets in the plane. For the construction and significance of potential flows the reader may consult [37]. For the nonlinear term holds $(\mathbf{u} \cdot \nabla)\mathbf{u} = 1/2\nabla(\mathbf{u}^2)$. Looking at the weak formulation of this term, it holds for all $\mathbf{v} \in \mathbf{V}^0$

$$\int_\Omega (\mathbf{u} \cdot \nabla)\mathbf{u} \cdot \mathbf{v} \, dx = \int_\Omega \nabla\left(\frac{\mathbf{u}^2}{2}\right) \cdot \mathbf{v} \, dx = -\int_\Omega \left(\frac{\mathbf{u}^2}{2}\right) \text{div}\,\mathbf{v} \, dx = 0.$$

This orthogonality may not hold in the discrete case, so similar as for the modified Stokes problem (2.13), a non-standard discretization of the nonlinear convection term is proposed that employs the reconstruction $\mathcal{R}_h$ in the velocity test functions

$$\int_\Omega (\mathbf{u}_h \cdot \nabla)\mathbf{u}_h \cdot \mathcal{R}_h\mathbf{v}_h \, dx.$$

In Tables 6 and 7 one can see the differences in the errors, when standard or non-standard discretizations of the nonlinear convection term are used in case of Taylor–Hood elements of order $k = 2, 3, 4$ on two consecutive meshes with 352 and 1408 elements. Note that for $k = 4$ the exact solution satisfies $\mathbf{u} \in \mathbf{V}_h$, but only for the non-standard discretization the velocity error vanishes. Similar to the Stokes example 6.1 we see that a mesh refinement does not heal the observed problems.

#dof	$\|\mathbf{u} - \mathbf{u}_h\|_{H^1}$	eoc	$\|\mathbf{u} - \mathbf{u}_h\|_{L^2}$	eoc	$\|p - p_h\|_{L^2}$	eoc
72	$5.27 \cdot 10^{-2}$		$5.01 \cdot 10^{-3}$		0.11	
252	$2.58 \cdot 10^{-2}$	1.032	$1.44 \cdot 10^{-3}$	1.794	$4.2 \cdot 10^{-2}$	1.418
948	$1.28 \cdot 10^{-2}$	1.007	$3.9 \cdot 10^{-4}$	1.890	$1.17 \cdot 10^{-2}$	1.838
3,684	$6.27 \cdot 10^{-3}$	1.033	$9.75 \cdot 10^{-5}$	1.998	$3.03 \cdot 10^{-3}$	1.955
14,532	$3.09 \cdot 10^{-3}$	1.021	$2.41 \cdot 10^{-5}$	2.016	$7.63 \cdot 10^{-4}$	1.988

Table 4: Errors for the modified lowest-order mini finite element method in Section 6.1.

#dof	$\|\mathbf{u} - \mathbf{u}_h\|_{H^1}$	eoc	$\|\mathbf{u} - \mathbf{u}_h\|_{L^2}$	eoc	$\|p - p_h\|_{L^2}$	eoc
115	$3.48 \cdot 10^{-3}$		$2.35 \cdot 10^{-4}$		0.15	
603	$2.07 \cdot 10^{-3}$	0.745	$1.18 \cdot 10^{-4}$	0.992	$8.03 \cdot 10^{-2}$	0.866
3,913	$6.38 \cdot 10^{-4}$	1.701	$1.79 \cdot 10^{-5}$	2.717	$2.21 \cdot 10^{-2}$	1.859
28,269	$1.87 \cdot 10^{-4}$	1.772	$2.53 \cdot 10^{-6}$	2.828	$5.54 \cdot 10^{-3}$	1.998
$2.15 \cdot 10^5$	$4.86 \cdot 10^{-5}$	1.942	$3.25 \cdot 10^{-7}$	2.958	$1.38 \cdot 10^{-3}$	2.005

Table 5: Errors for the modified Taylor–Hood finite element method of order $k = 2$ in Section 6.2.

7. Appendix.

THEOREM 20. *For $\Omega \subseteq \mathbb{R}^3$, $V \in \Omega$ and $k \geq 0$ it holds*

$$\{\kappa_{\vec{x}-V}(\boldsymbol{q}_1) : \boldsymbol{q}_1 \in [\Pi^k(\Omega)]^3\} = \{\kappa_{\vec{x}-V}(\boldsymbol{q}_2) : \boldsymbol{q}_2 \in [\Pi^k(\Omega)]^3, \operatorname{div} \boldsymbol{q}_2 = 0\}$$

Proof. Without loss of generality we can set $V = \mathbf{0}$. For $k = 0$ there is nothing to prove. In the case $k \geq 1$, for $\mathbf{q}_1 \in [\Pi^k(\Omega)]^3$ we define

$$\mathbf{q}_2 := \mathbf{q}_1 + \vec{x}w$$

with $w \in \Pi^{k-1}(\Omega)$. Note that

(7.1) $$\kappa_{\vec{x}}(\mathbf{q}_2) = \vec{x} \times \mathbf{q}_2 = \vec{x} \times \mathbf{q}_1 + \underbrace{\vec{x} \times \vec{x}}_{=\mathbf{0}} w = \kappa_{\vec{x}}(\mathbf{q}_1),$$

and

$$\operatorname{div} \mathbf{q}_2 = \operatorname{div}(\mathbf{q}_1 + \vec{x}w) = \operatorname{div} \mathbf{q}_1 + \operatorname{div}(\vec{x})w + \vec{x} \cdot \nabla w = \operatorname{div} \mathbf{q}_1 + 3w + \vec{x} \cdot \nabla w.$$

As we want to have $\operatorname{div} \mathbf{q}_2 = 0$, we have to solve the equation

(7.2) $$3w + \vec{x} \cdot \nabla w = -\operatorname{div} \mathbf{q}_1.$$

Due to the finite dimensionality of $\Pi^{k-1}(\Omega)$, this linear inhomogeneous equation can be solved, if we show that from

(7.3) $$3w + \vec{x} \cdot \nabla w = 0 \quad \text{it follows} \quad \Rightarrow w = 0.$$

without reconstruction				
k	#dof	$\|\mathbf{u} - \mathbf{u}_h\|_{H^1}$	$\|\mathbf{u} - \mathbf{u}_h\|_{L^2}$	$\|p - p_h\|_{L^2}$
2	1,748	1.42	$2.21 \cdot 10^{-2}$	0.27
3	4,132	$8.91 \cdot 10^{-2}$	$9.02 \cdot 10^{-4}$	$1.25 \cdot 10^{-2}$
4	7,572	$1.33 \cdot 10^{-3}$	$7.4 \cdot 10^{-6}$	$2.49 \cdot 10^{-4}$

with reconstruction				
k	#dof	$\|\mathbf{u} - \mathbf{u}_h\|_{H^1}$	$\|\mathbf{u} - \mathbf{u}_h\|_{L^2}$	$\|p - p_h\|_{L^2}$
2	1,748	$8.5 \cdot 10^{-2}$	$8.08 \cdot 10^{-4}$	0.26
3	4,132	$9.76 \cdot 10^{-4}$	$7.39 \cdot 10^{-6}$	$1.48 \cdot 10^{-2}$
4	7,572	$3.66 \cdot 10^{-12}$	$1.66 \cdot 10^{-14}$	$4.94 \cdot 10^{-4}$

Table 6: Errors for the Taylor–Hood and the modified Taylor–Hood finite element method for the Navier–Stokes example $|\mathcal{T}| = 352$

without reconstruction				
k	#dof	$\|\mathbf{u} - \mathbf{u}_h\|_{H^1}$	$\|\mathbf{u} - \mathbf{u}_h\|_{L^2}$	$\|p - p_h\|_{L^2}$
2	6,600	0.39	$2.91 \cdot 10^{-3}$	$6.55 \cdot 10^{-2}$
3	16,004	$1.25 \cdot 10^{-2}$	$6.56 \cdot 10^{-5}$	$1.59 \cdot 10^{-3}$
4	29,572	$8.29 \cdot 10^{-5}$	$2.27 \cdot 10^{-7}$	$1.56 \cdot 10^{-5}$

with reconstruction				
k	#dof	$\|\mathbf{u} - \mathbf{u}_h\|_{H^1}$	$\|\mathbf{u} - \mathbf{u}_h\|_{L^2}$	$\|p - p_h\|_{L^2}$
2	6,600	$2.12 \cdot 10^{-2}$	$1.04 \cdot 10^{-4}$	$6.46 \cdot 10^{-2}$
3	16,004	$1.2 \cdot 10^{-4}$	$4.55 \cdot 10^{-7}$	$1.88 \cdot 10^{-3}$
4	29,572	$4.28 \cdot 10^{-12}$	$9.59 \cdot 10^{-15}$	$2.99 \cdot 10^{-5}$

Table 7: Errors for the Taylor–Hood and the modified Taylor–Hood finite element method for the Navier–Stokes example with $|\mathcal{T}| = 1408$

For $k = 1$ it holds $w \in \Pi^0(\Omega)$ and $\mathbf{q}_1 \in [\Pi^1(\Omega)]^3$ and the statement is obviously true. In the case $k \geq 2$ we use the following representation of w

$$w(x, y, z) = \tilde{w}(x, y, z) + \sum_{i=0}^{k-1} \sum_{j=0}^{k-1-i} c_{ij} x^i y^j z^{k-1-i-j},$$

with $\tilde{w} \in \Pi^{k-2}(\Omega)$. Using assumption (7.3) and $3\tilde{w} + \vec{x} \cdot \nabla \tilde{w} =: \hat{w} \in \Pi^{k-2}(\Omega)$ we now

22

have

$$3w + \vec{x} \cdot \nabla w = \hat{w} + \sum_{i=0}^{k-1} \sum_{j=0}^{k-1-i} (k-1)c_{ij}x^i y^j z^{k-1-i-j} = 0$$

$$\forall (x, y, z) \in \Omega,$$

what leads to $c_{ij} = 0 \; \forall i, j$ and so $\hat{w} = 3\tilde{w} + \vec{x} \cdot \nabla \tilde{w} = 0$. By induction it follows $w = 0$. Therefore, we can solve equation (7.2) and for every $\mathbf{q}_1$ we find a $\mathbf{q}_2$ with div $\mathbf{q}_2 = 0$ and due to (7.1) the theorem is shown. $\square$

REFERENCES

[1] D. N. ARNOLD, F. BREZZI, AND M. FORTIN, *A stable finite element for the Stokes equations*, Calcolo, 21 (1984), pp. 337–344 (1985).

[2] D. N. ARNOLD, R. S. FALK, AND R. WINTHER, *Finite element exterior calculus, homological techniques, and applications*, Acta Numerica, 15 (2006), pp. 1–155.

[3] J. AUBIN, *Approximation of elliptic boundary-value problems*, Pure and applied mathematics, Wiley-Interscience, 1972.

[4] D. BOFFI, M. FORTIN, AND F. BREZZI, *Mixed finite element methods and applications*, Springer series in computational mathematics, Springer, Berlin, Heidelberg, 2013.

[5] D. BRAESS AND J. SCHÖBERL, *Equilibrated residual error estimator for edge elements*, Math. Comp., 77 (2008), pp. 651–672.

[6] C. BRENNECKE, A. LINKE, C. MERDON, AND J. SCHÖBERL, *Optimal and pressure-independent L^2 velocity error estimates for a modified Crouzeix-Raviart Stokes element with BDM reconstructions*, J. Comput. Math., 33 (2015), pp. 191–208.

[7] F. BREZZI, J. DOUGLAS, AND L. D. MARINI, *Two families of mixed finite elements for second order elliptic problems*, Numerische Mathematik, 47 (1985), pp. 217–235.

[8] P. DESTUYNDER AND B. MÉTIVET, *Explicit error bounds in a conforming finite element method*, Math. Comp., 68 (1999), pp. 1379–1396.

[9] D. A. DI PIETRO, A. ERN, A. LINKE, AND F. SCHIEWECK, *A discontinuous skeletal method for the viscosity-dependent Stokes problem*, Comput. Methods Appl. Mech. Engrg., 306 (2016), pp. 175–195.

[10] O. DOROK, W. GRAMBOW, AND L. TOBISKA, *Aspects of finite element discretizations for solving the Boussinesq approximation of the Navier–Stokes Equations*, Notes on Numerical Fluid Mechanics: Numerical Methods for the Navier-Stokes Equations., 47 (1994), pp. 50–61.

[11] R. G. DURÁN AND A. L. LOMBARDI, *Error estimates for the raviartthomas interpolation under the maximum angle condition*, SIAM Journal on Numerical Analysis, 46 (2008), pp. 1442–1453.

[12] A. ERN AND J.-L. GUERMOND, *Finite element quasi-interpolation and best approximation*, ArXiv e-prints, (2015), arXiv:1505.06931.

[13] R. S. F. F. BREZZI, *Stability of higher-order Hood-Taylor method*, SIAM J. Numer. Anal., 28 (1991).

[14] R. S. FALK AND R. WINTHER, *The bubble transform: A new tool for analysis of finite element methods*, Foundations of Computational Mathematics, 16 (2016), pp. 297–328.

[15] L. FRANCA AND T. HUGHES, *Two classes of mixed finite element methods*, Computer Methods in Applied Mechanics and Engineering, 69 (1988), pp. 89–129.

[16] G. FU, Y. JIN, AND W. QIU, *Parameter-free superconvergent $H(\text{div})$-conforming HDG methods for the Brinkman equations*, ArXiv e-prints, (2016), arXiv:1607.07662.

[17] K. GALVIN, A. LINKE, L. REBHOLZ, AND N. WILSON, *Stabilizing poor mass conservation in incompressible flow problems with large irrotational forcing and application to thermal convection*, Comput. Methods Appl. Mech. Engrg., 237/240 (2012), pp. 166–176.

[18] J.-F. GERBEAU, C. LE BRIS, AND M. BERCOVIER, *Spurious velocities in the steady flow of an incompressible fluid subjected to external forces*, International Journal for Numerical Methods in Fluids, 25 (1997), pp. 679–695.

[19] V. GIRAULT AND P.-A. RAVIART, *Finite Element Methods for Navier-Stokes Equations*, vol. 5 of Springer Series in Computational Mathematics, Springer-Verlag, Berlin, 1986.

[20] B. GMEINER, C. WALUGA, AND B. WOHLMUTH, *Local mass-corrections for continuous pressure approximations of incompressible flow*, SIAM J. Numer. Anal., 52 (2014), pp. 2931–2956.

[21] J. GUZMÁN AND M. NEILAN, *Conforming and divergence-free Stokes elements in three dimensions*, IMA J. Numer. Anal., 34 (2014), pp. 1489–1508.

[22] J. Guzmán and M. Neilan, *Conforming and divergence-free Stokes elements on general triangular meshes*, Math. Comp., 83 (2014), pp. 15–36.

[23] V. John, A. Linke, C. Merdon, M. Neilan, and L. Rebholz, *On the divergence constraint in mixed finite element methods for incompressible flows*, SIAM Review, accepted (2016).

[24] P. Lederer, *Pressure-robust discretizations for Navier–Stokes equations: Divergence-free reconstruction for Taylor–Hood elements and high order Hybrid Discontinuous Galerkin methods*, master's thesis, Vienna Technical University, 2016.

[25] C. Lehrenfeld and J. Schöberl, *High order exactly divergence-free Hybrid Discontinuous Galerkin Methods for unsteady incompressible flows*, Comput. Methods Appl. Mech. Engrg., 307 (2016), pp. 339–361.

[26] A. Linke, *A divergence-free velocity reconstruction for incompressible flows*, C. R. Math. Acad. Sci. Paris, 350 (2012), pp. 837–840.

[27] A. Linke, *On the role of the Helmholtz decomposition in mixed methods for incompressible flows and a new variational crime*, Comput. Methods Appl. Mech. Engrg., 268 (2014), pp. 782–800.

[28] A. Linke, G. Matthies, and L. Tobiska, *Robust arbitrary order mixed finite element methods for the incompressible Stokes equations with pressure independent velocity errors*, ESAIM: M2AN, 50 (2016), pp. 289–309.

[29] A. Linke and C. Merdon, *On velocity errors due to irrotational forces in the Navier–Stokes momentum balance*, Journal of Computational Physics, 313 (2016), pp. 654–661.

[30] A. Linke, C. Merdon, and W. Wollner, *Optimal L^2 velocity error estimate for a modified pressure-robust Crouzeix-Raviart Stokes element*, IMA Journal of Numerical Analysis, (2016), doi:10.1093/imanum/drw019, http://imajna.oxfordjournals.org/content/early/2016/05/17/imanum.drw019.abstract.

[31] K.-A. Mardal, J. Schöberl, and R. Winther, *A uniformly stable Fortin operator for the Taylor-Hood element*, Numer. Math., 123 (2013), pp. 537–551.

[32] J. Nitsche, *Ein Kriterium für die Quasi-Optimalität des Ritzschen Verfahrens*, Numerische Mathematik, 11 (1968), pp. 346–348.

[33] M. Olshanskii and A. Reusken, *Grad-div stabilization for Stokes equations*, Math. Comp., 73 (2004), pp. 1699–1718.

[34] M. A. Olshanskii, G. Lube, T. Heister, and J. Löwe, *Grad-div stabilization and subgrid pressure models for the incompressible Navier-Stokes equations*, Comput. Methods Appl. Mech. Engrg., 198 (2009), pp. 3975–3988.

[35] P. Oswald, *On a BPX preconditioner for P_1 elements*, Computing, 51 (1993), pp. 125–133.

[36] J. M. T. P. A. Raviart, *Primal hybrid finite element methods for 2nd order elliptic equations*, Mathematics of Computation, 31 (1977), pp. 391–413.

[37] L. Prandtl, *Prandtl—Essentials of fluid mechanics*, vol. 158 of Applied Mathematical Sciences, Springer, New York, third ed., 2010.

[38] J. Qin, *On the convergence of some low order mixed finite elements for incompressible fluids*, PhD thesis, Pennsylvania State University, 1994.

[39] J. Schöberl, *NETGEN An advancing front 2D/3D-mesh generator based on abstract rules*, Computing and Visualization in Science, 1 (1997), pp. 41–52.

[40] J. Schöberl, *C++11 Implementation of Finite Elements in NGSolve*, Institute for Analysis and Scientific Computing, Vienna University of Technology, (2014).

[41] J. Schöberl, J. M. Melenk, C. Prechstein, and S. Zaglmayr, *Additive Schwarz preconditioning for p-version triangular and tetrahedral finite elements*, IMA Journal of Numerical Analysis, 28 (2007), pp. 1–24.

[42] R. Verfürth, *Error estimates for a mixed finite element approximation of the Stokes equations*, RAIRO Anal. Numér., 18 (1984), pp. 175–182.

[43] R. Verfürth, *A Posteriori Error Estimation Techniques for Finite Element Methods.*, Oxford University Press, Oxford, 2013.

[44] S. Zhang, *A new family of stable mixed finite elements for the 3d Stokes equations*, Math. Comp., 74 (2005), pp. 543–554.

[45] S. Zhang, *A family of $Q_{k+1,k} \times Q_{k,k+1}$ divergence-free finite elements on rectangular grids*, SIAM J. Numer. Anal., 47 (2009), pp. 2090–2107.